strains. Funding was provided by the Sandler Research Fellowship (G.S.-O.), the Program for Breakthrough Biomedical Research at the University of California, San Francisco (U.H.), and NIH–National Institute on Alcohol Abuse and Alcoholism (U.H.). The authors declare that they have no competing interests. A detailed description of all materials and methods as well as supplementary figures are available as supporting online material.

Supporting Online Material
www.sciencemag.org/cgi/content/full/335/6074/1351/DC1
Materials and Methods
Figs. S1 to S6
References

28 October 2011; accepted 26 January 2012
10.1126/science.1215932

SNARE Proteins: One to Fuse and Three to Keep the Nascent Fusion Pore Open

Lei Shi,[1] Qing-Tao Shen,[2] Alexander Kiel,[1] Jing Wang,[1] Hong-Wei Wang,[2] Thomas J. Melia,[1] James E. Rothman,[1]* Frédéric Pincet[1,3]*

Neurotransmitters are released through nascent fusion pores, which ordinarily dilate after bilayer fusion, preventing consistent biochemical studies. We used lipid bilayer nanodiscs as fusion partners; their rigid protein framework prevents dilation and reveals properties of the fusion pore induced by SNARE (soluble *N*-ethylmaleimide–sensitive factor attachment protein receptor). We found that although only one SNARE per nanodisc is required for maximum rates of bilayer fusion, efficient release of content on the physiologically relevant time scale of synaptic transmission apparently requires three or more SNARE complexes (SNAREpins) and the native transmembrane domain of vesicle-associated membrane protein 2 (VAMP2). We suggest that several SNAREpins simultaneously zippering their SNARE transmembrane helices within the freshly fused bilayers provide a radial force that prevents the nascent pore from resealing during synchronous neurotransmitter release.

Efficient synaptic transmission requires the fast release of neurotransmitters from synaptic vesicles that fuse with the presynaptic plasma membrane upon entry of calcium ions (*1*). Membrane fusion necessarily implies a fusion pore that opens between the vesicle and its partner membrane at the instant of fusion. The conductance properties of such nascent fusion pores suggest that their typical diameters are in the range of ~2 nm, although considerable variability exists (*2*–*5*). Neurotransmitter is released from synaptic vesicles [diameter ~40 nm (*6*, *7*)] by diffusion through the nascent pore in the first 100 to 200 μs, even before appreciable dilation of the pore occurs (*4*). The transient and variable nature of the fusion pore has severely limited biochemical and physical chemical studies.

We suggest that nanodiscs (*8*–*11*) provide an ideal model for such studies because the small amount of disc lipid will suffice to allow pores to open but not expand (Fig. 1 and Fig. 2A) beyond their nascent, physiologically relevant state for neurotransmitter release. Nanodiscs are synthetic lipoprotein particles that contain a small piece of circular lipid bilayer (up to ~17 nm in diameter) wrapped by two copies of membrane scaffold protein (MSP) derived from apolipoprotein A1. In the system we describe here, nanodiscs contain the synaptic vesicle SNARE (v-SNARE) VAMP2 and small unilamellar vesicles [diameter 30 to 60 nm (*12*)] contain the synaptic target membrane SNARE (t-SNARE) complex of syntaxin 1 and SNAP25. SNAREs are the core machinery for this and other cellular membrane fusion processes (*12*–*14*). They assemble between bilayers as a four-helix bundle (*15*) that imparts sufficient force to cause bilayer fusion (*16*).

After reconstitution (supplementary text), the nanodiscs containing VAMP2 (v-discs) were separated by gel filtration (Fig. 1, A to C). Each disc contained about 400 lipid molecules wrapped by two MSPs. With a starting VAMP2/MSP ratio of 6:2, we recovered ~7 VAMP2 copies per disc on average after removing VAMP2-free dics. Electron microscopy of v-discs confirmed an average diameter of 16 ± 2 nm (Fig. 1D). Not surprisingly, single VAMP2 proteins on these discs could not be readily distinguished because of their small size and flexible structure. However, addition of the soluble t-SNARE (a complex of syntaxin H3 cytosolic domain and SNAP25N/C helical domains) formed rodlike SNARE complexes that were seen to protrude from the nanodiscs (Fig. 1D). This confirms that VAMP2 on nanodiscs can form SNARE complexes.

We used a well-established lipid mixing assay (*17*) to test whether v-discs can fuse with t-vesicles. Nitro-2-1,3-benzoxadiazol-4-yl-phosphatidylethanolamine (NBD-PE) and rhodamine-PE were included in the v-discs (1.5 mol % each). This surface concentration of rhodamine effectively quenches the NBD fluorescence. However, when a nanodisc fuses with a liposome, NBD fluorescence will greatly increase because of the substantial (>50-fold) lipid dilution as the disc lipid mixes with the massive excess of vesicle lipid, as we observed (Fig. 2B). Little or no increase of NBD signal was observed in control experiments. The slow lipid mixing between nanodiscs and vesicles was limited by the rate of docking (initial SNARE assembly) and not by the rate of fusion (fig. S1), as is the case for vesicle-vesicle fusion systems (*18*). A similar fusion process was observed when the SNAREs were placed in the opposite topology, with v-SNAREs in the vesicle and t-SNAREs in the nanodisc (fig. S2).

To monitor efflux of content via fusion pores that necessarily form at least transiently during the fusion process, we encapsulated calcium (50 mM) in the liposomes, which were then incubated with v-discs in a medium containing a calcium-activated fluorophore, Mag-Fluo-4 (2 μM, K_d for calcium = 22 μM; Invitrogen). When pores open, calcium diffuses through the pores into the exterior buffer, inducing a fluorescence signal. The results (Fig. 2C) clearly show that calcium was released in a SNARE-specific manner. To ascertain that this efflux was due to diffusion through a pore, rather than transient lysis or leakage of the vesicle during fusion, we tested the rate of release of vesicle cargos of different sizes—specifically, the calcium chelator EDTA (Stokes radius, ~0.4 nm) and EGTA (Stokes radius, ~0.5 nm). EDTA release from liposomes was faster than EGTA release from liposomes by a factor of 2.3 (fig. S3). From these data, a pore size of ~2 nm can be calculated (supplementary text), similar in size to the nascent fusion pore size calculated from electrophysiological measurements (*3*).

When vesicles fuse to target membranes, the fusion pore eventually expands and the vesicle is incorporated into the target membrane. With nanodiscs, however, the pore cannot appreciably expand beyond its nascent diameter of ~2 nm, so the only means available to reduce membrane stress (resulting from the extreme curvature inherent in a small pore) is for the pore to eventually reseal. To confirm the prediction that nanodisc-vesicle pores reseal, we introduced dithionite (5 mM) into samples 40 min after beginning the fusion assay. Dithionite quenches all externally accessible NBD (*19*), including NBD on both faces of unreacted nanodiscs and NBD-PE that had diffused into the outer leaflets of liposomes via hemifusion or full fusion. Dithionite is also small enough (Stokes radius, 0.2 to 0.3 nm) to readily diffuse through any 2-nm fusion pores that may remain open and quench the NBD signal on the inner leaflets in the case that the pore remains open, but will not gain access to the interior if the pore has (as predicted) closed off. We observed that some of the NBD dye remained protected against dithionite, and only

[1]Department of Cell Biology, School of Medicine, Yale University, New Haven, CT 06520, USA. [2]Department of Molecular Biophysics and Biochemistry, Yale University, New Haven, CT 06520, USA. [3]Laboratoire de Physique Statistique, UMR CNRS 8550 associée aux Universités Paris 6 et Paris 7, Ecole Normale Supérieure, 24 rue Lhomond, 75005 Paris, France.

*To whom correspondence should be addressed. E-mail: james.rothman@yale.edu (J.E.R.); pincet@lps.ens.fr (F.P.)

after the fusion reaction (Fig. 2D and fig. S4). No NBD protection was found for the negative controls. Thus, there are some fusion events that correspond to full fusion between the nanodisc and the liposome, in which a pore must have opened and then resealed. Reverse experiments where NBD-PE was initially only on the t-liposomes confirmed that essentially no pores remained open after full fusion (fig. S5). The dithionate data indicate that ~ 50% of all fusion events entailed full fusion with subsequent resealing of the pore (see supplementary text). The ~50% balance of SNARE complex–dependent events can be accounted for by events resembling hemifusion in which no pore opens and only the outer leaflets are shared between the liposome and nanodisc. In all cases, the nanodisc remained attached to the liposomes after the pore resealed (fig. S6, A to D), consistent with the idea that after full fusion, the pore reseals to a hemifusion-like state in which a stalk of lipid bilayer permanently connects the outer leaflet of the vesicle to what had been the SNARE complex–containing leaflet of the nanodisc (fig. S6F). After resealing, VAMP2 is fully resistant to toxin cleavage, which suggests that it is in cis-SNARE complexes (fig. S6, E and F).

The number of VAMP2 copies per disc can be controlled by adjusting the input VAMP2/MSP ratio. With increasing VAMP2/MSP ratios during assembly of nanodiscs, the v-disc products eluted progressively earlier on gel filtration columns (Superdex 200), consistent with increasing size and more VAMP2 being inserted into each disc (Fig. 3A). To test how the number of SNAREpins affects fusion, we purified seven sets of nanodiscs containing, respectively, an average of 1.2 (ND1), 2.2 (ND2), 3.15 (ND3), 4.3 (ND4), 5.5 (ND5), 7.4 (ND7), and 9.3 (ND9) copies of VAMP2 after VAMP2-free nanodiscs were removed by affinity purification (Fig. 3B and fig. S7). VAMP2 and MSP were mixed in these preparations in different proportions, and the VAMP2/MSP ratios in the final isolated nanodiscs used in the fusion experiments were established by three independent

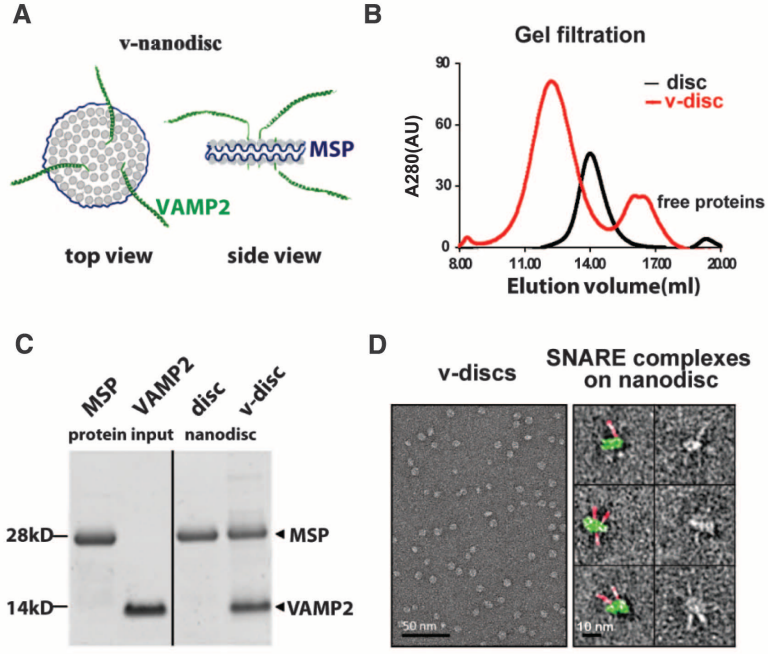

Fig. 1. (**A**) Cartoon showing the v-disc model. The nanodisc is a small piece of lipid bilayer wrapped by two MSPs (blue). VAMP2 (green) can insert into a nanodisc to form a v-disc (*11*). The lipid head groups are shown as gray spheres. (**B**) Elution profile of nanodisc or v-disc on Superdex 200 10/300 GL column. Embedment of VAMP2 results in the earlier elute volume of a v-disc (red major peak) relative to that of a VAMP2-free nanodisc (black peak). By gel filtration, the 6×His-SUMO tag (cleaved from VAMP2 by SUMO-protease, the red minor peak) can also be removed. (**C**) SDS–polyacrylamide gel electrophoresis (PAGE) gel stained with Coomassie Brilliant Blue showing the input and final nanodisc products after gel filtration. (**D**) V-disc samples were analyzed in an FEI Tecnai-12 electron microscope. Left panel: V-discs show regular "disc" shapes; VAMP2 protein can hardly be seen because of small protein size and flexible structure. Right panel: When soluble syntaxin 1A H3 domain and SNAP-25N/C domain were co-incubated with v-disc, they form SNARE complexes that can be seen as rodlike structures (red) protruding from two sides of the v-disc (green).

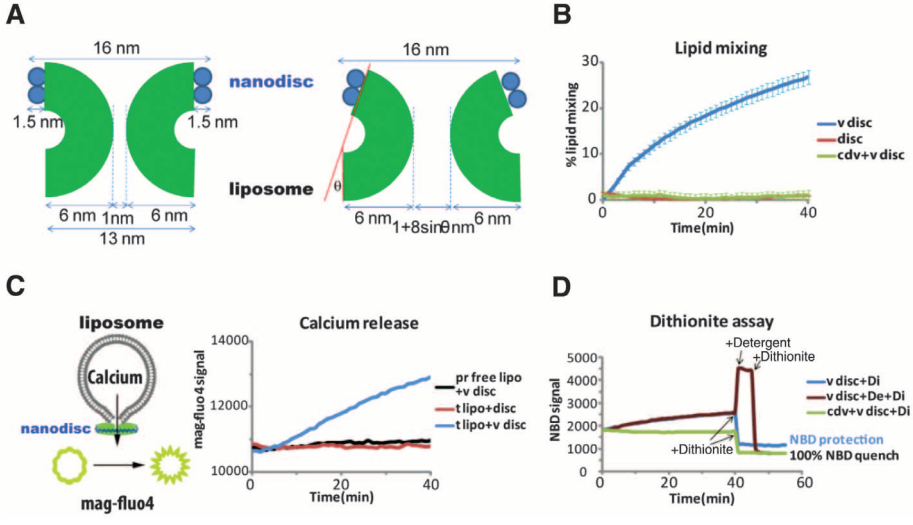

Fig. 2. (**A**) Schematics showing how the fusion pore can be envisioned. The diameter of the nanodisc is 16 nm. Lipids that naturally form flat surfaces will favor structures that have a zero net curvature (when neglecting the Gaussian curvature). Hence, in neck-like structures, the negative curvatures (shown here as perpendicular to the pore) are of the same order; likewise, for saddle-like structures, the positive (pore) curvatures are of the same order. A 4-nm pore would correspond to a 6-nm curvature for the exterior of the bilayer. This is approximately what is represented here. With no stress, a 1-nm pore can form. With a reasonable amount of stress (θ = 20°), a 4-nm pore diameter would result. (**B**) Lipid mixing is SNARE-specific. V-discs exchanged lipids with t-liposomes (blue). Discs without VAMP2 do not fuse with t-liposomes (red); cytoplasmic domain of VAMP2 (CDV), which titrates the free t-SNARE, also blocks the fusion (green). (**C**) Calcium release is SNARE-specific. Calcium (50 mM) is encapsulated into t-liposome; during the liposome-nanodisc fusion, the pore opens, calcium is released from the liposome to the exterior buffer, and the Mag-Fluo-4 signal is enhanced. An increasing Mag-Fluo-4 signal indicates that calcium is continuously released during the fusion (blue); limited calcium release is observed under nonfusogenic conditions (red and black). (**D**) Dithionite assay showed some NBD protection after 40 min of fusion (blue). To completely quench all NBD signal, detergent (De) was first added to disrupt the liposomes, followed by dithionite (Di) to obtain 100% quench (brown). With CDV to block the fusion, no NBD protection was observed after dithionite treatment (green).

methods: Coomassie Blue–based protein determinations (Fig. 3B), quantitative Western blotting (fig. S7), and counting of the discrete photobleaching steps of single nanodisc particles containing fluorescently labeled VAMP2 (fig. S13). The three methods agreed very closely [within ±3% (SD/mean × 100) for ND1 and ND2 in particular; see table S2].

Remarkably, all seven samples drove lipid mixing at the same rate (Fig. 3C), which implies that a single v-SNARE per nanodisc yields the maximum rate of membrane fusion. Furthermore, the dithionite protection assay shows that for any VAMP2 copy number, the percentage of lipid-mixing events corresponding to full fusion remains unchanged at 45 ± 7% (SD; fig. S8). Together, these two results clearly establish that a single SNAREpin is sufficient to drive complete membrane fusion.

The pores forming in our nanodisc-liposome system are transient, eventually resealing of their own accord (fig. S5). Because our lipid-mixing experiments result in full membrane fusion (i.e., full exchange of lipid), we can set a lower limit for how long these pores must have remained open. In order for all of the fluorescent phospholipid to equilibrate between the nanodisc and the liposome, the pore must remain open for ~10 μs (it takes ~10 μs for a phospholipid with a diffusion coefficient of 5 $\mu m^2/s$ to cover 50 nm^2, half of a nanodisc embedded bilayer, and reach the fusion pore). In contrast, simple considerations and in vivo observations of neurotransmitter release from synaptic vesicles suggest that a much longer time (~100 μs) is required for full efflux of the content with similar size as neurotransmitter from ~40-nm liposomes or synaptic vesicles (*4*, *20*–*22*).

Do the fusion pores between nanodiscs and vesicles remain open long enough for such cargo to efflux? The answer (Fig. 3D) is that they do when several or more SNARE complexes can form, but not when only a single SNAREpin is available. In contrast to the rate of lipid mixing, maximum cargo efflux decreased precipitously from 12% (ND9 and ND7) to less than 2% (ND1 and ND2) as the number of VAMP2s per disc decreased from ~9 to ~1. Thus, even though the rate and frequency of full membrane fusion events do not depend on the number of VAMP2 molecules per disc, the efficiency of cargo release is highly sensitive to SNAREpin number, increasing markedly as the number of SNAREpins increases above two per disc.

At very low SNARE numbers (i.e., ND1 or ND2), the pore opens only long enough to exchange lipid, and thus only a small fraction of the content is released. The amount of release increases starting with ND3 discs and reaches a maximum with ND7 discs, which reconstituted with about 7 VAMP2 proteins total or about 3.5 per nanodisc face (table S2); this finding suggests that maximum efflux requires 3 or 4 VAMP2 proteins. The simplest model is that a limited content release occurs when one SNAREpin is engaged, whereas a sudden increase in content release occurs above a threshold when enough SNAREpins are involved (fig. S12C). In the nanodisc system, that critical number is achieved when any one side of the nanodisc has at least the minimum necessary number of SNAREs. Indeed, if we assume that the VAMP2 distributes randomly between the two sides of each disc (fig. S12B), the calcium release across the whole of the titration fits well to such a "cooperative" model and describes the threshold number of SNAREpins for efficient content release as ~3 (fig. S12C), which is consistent with in vivo observations.

The role of the SNARE transmembrane domains (TMDs) in fusion has been unclear. Membrane anchorage of the assembling cytosolic domains of VAMP2 and syntaxin is needed, and when this is provided by membrane-spanning lipids, fusion still occurs (*17*). In absolute contrast, point mutations in the syntaxin 1 TMD reduce the amplitude of the foot signal in electrophysiology (*23*), and deletion in the VAMP2 TMD significantly reduces neurotransmitter release (*24*). This implies a role for the TMDs either in the opening of the nascent physiological fusion pore, or in maintaining it open for the ~100 μs needed for transmitter efflux, or both. Because fusion pores must open (at least transiently) when lipid anchors mediate fusion, the simplest possibility is that the TMDs somehow keep the fusion pore from resealing when transmitter is exiting and the pore has not begun to appreciably expand. In this connection, it is noteworthy that the VAMP2 and syntaxin TMDs extend as a two-helix bundle through the entire span of the membrane (*25*). This raises the possibility that force resulting from the terminal zippering of SNARE TMDs within the bilayer could provide a source of energy to tip the balance against resealing in the nascent fusion pore.

To test this hypothesis, we used three chimeric VAMP2 proteins in which the VAMP2 TMD was replaced by (i) a dioleoyl phospholipid that spans only one monolayer (C18), (ii) a long C45 isoprenoid that can span the lipid bilayer (C45), or (iii) a non-SNARE TMD from platelet-derived growth factor receptor (PDGFR) (Fig. 4A). As with the wild-type VAMP2, seven samples of PDGFR-VAMP2-discs (characterized in fig. S9)

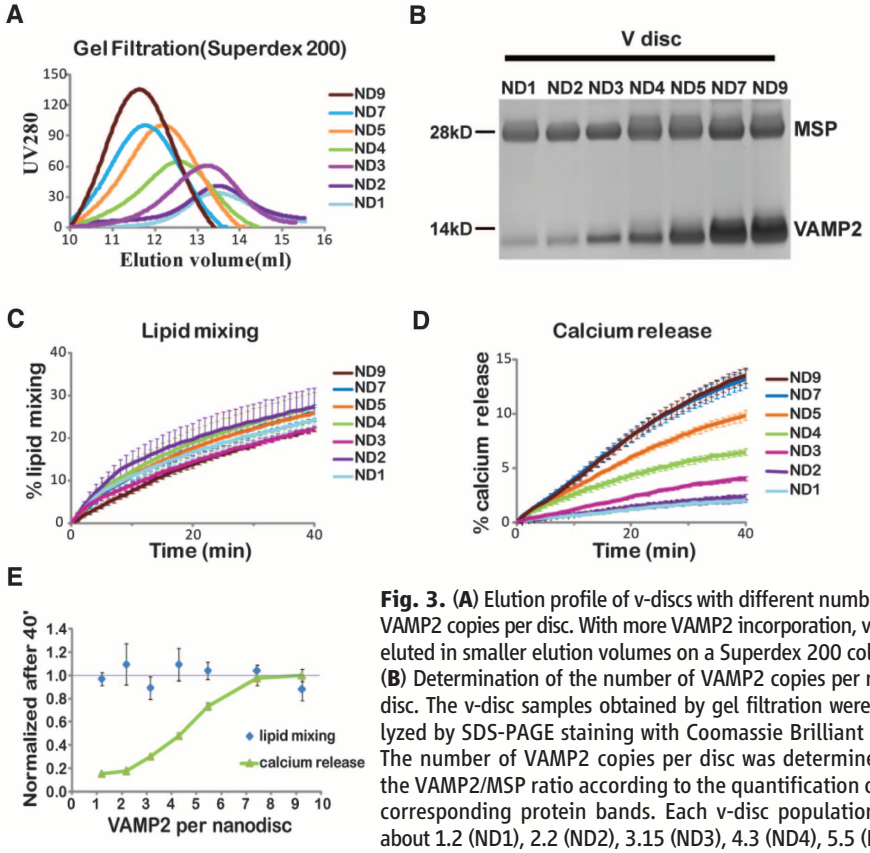

Fig. 3. (**A**) Elution profile of v-discs with different numbers of VAMP2 copies per disc. With more VAMP2 incorporation, v-discs eluted in smaller elution volumes on a Superdex 200 column. (**B**) Determination of the number of VAMP2 copies per nanodisc. The v-disc samples obtained by gel filtration were analyzed by SDS-PAGE staining with Coomassie Brilliant Blue. The number of VAMP2 copies per disc was determined by the VAMP2/MSP ratio according to the quantification of the corresponding protein bands. Each v-disc population has about 1.2 (ND1), 2.2 (ND2), 3.15 (ND3), 4.3 (ND4), 5.5 (ND5), 7.4 (ND7), and 9.3 (ND9) copies of VAMP2 per disc on average. (**C**) Lipid mixing assays demonstrate that discs with varying VAMP2 copy numbers are equally efficient in fusing with calcium-encapsulated t-liposomes. (**D**) Calcium release assay shows different kinetics when v-discs with different copy numbers of VAMP2 fuse with t-liposomes. Calcium release is gradually increased with higher copy numbers of VAMP2 inserted into the nanodiscs. The error bars are SEM. (**E**) The endpoint values after a 40-min fusion reaction are presented for both lipid mixing (blue) and calcium release (green). Lipid mixing, normalized by the average endpoint value, does not vary significantly with the number of VAMP2 copies. Calcium release, normalized by the value for ND9, varies as a sigmoid with an inflection point at ~5 VAMP2 copies per nanodisc.

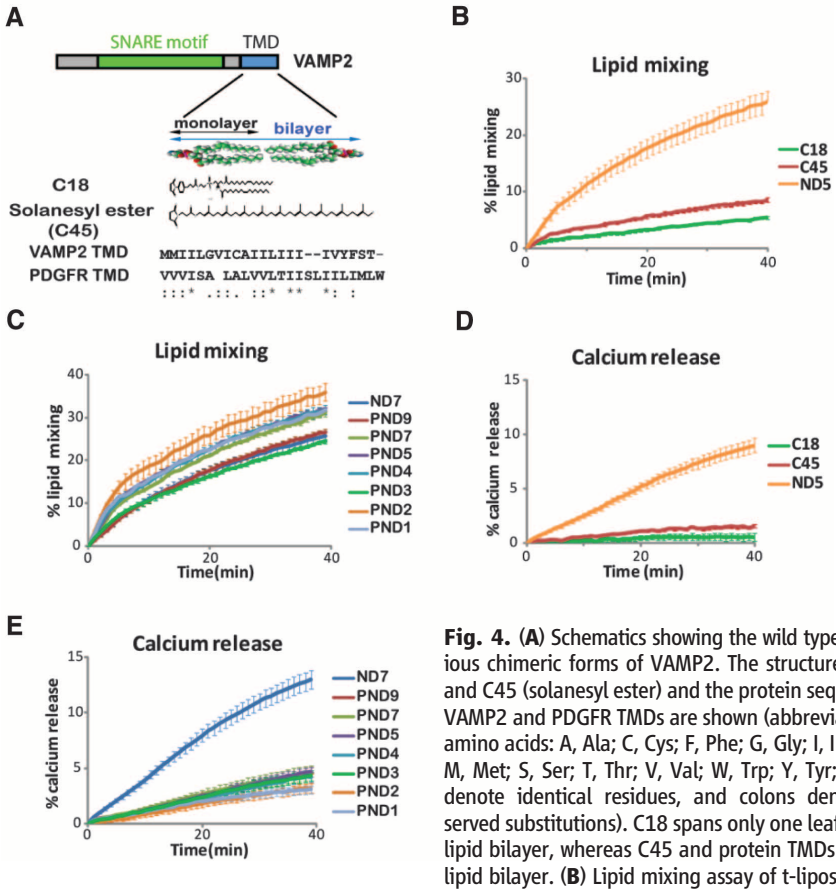

Fig. 4. (**A**) Schematics showing the wild type and various chimeric forms of VAMP2. The structures of C18 and C45 (solanesyl ester) and the protein sequences of VAMP2 and PDGFR TMDs are shown (abbreviations for amino acids: A, Ala; C, Cys; F, Phe; G, Gly; I, Ile; L, Leu; M, Met; S, Ser; T, Thr; V, Val; W, Trp; Y, Tyr; asterisks denote identical residues, and colons denote conserved substitutions). C18 spans only one leaflet of the lipid bilayer, whereas C45 and protein TMDs cross the lipid bilayer. (**B**) Lipid mixing assay of t-liposome with v-disc prepared with wild-type VAMP2 (ND5) or CDV with C18 or C45. The lipid anchor, either C18 or C45, shows compromised fusion efficiency relative to wild-type VAMP2 with native TMD. (**C**) Lipid mixing assay shows that the TMDs of VAMP2 and PDGFR have similar fusion kinetics, which suggests that these two TMDs are equivalent in lipid mixing. (**D**) Calcium release assay shows substantially reduced release when protein TMD is replaced by lipid anchor, either C18 or C45. (**E**) Calcium release assay reveals that VAMP2 TMD is more efficient than PDGFR TMD for content release. The error bars are SEM.

were prepared: PND9, PND7, PND5, PND4, PND3, PND2, and PND1, respectively containing an average of 9.0, 7.2, 5.7, 4.4, 3.75, 2.7, and 1.2 copies of PDGFR-VAMP2. Lipid anchors (C18 and C45, both with an average of ~5 copies per nanodisc) were less efficient for fusion than the VAMP2 TMD by a factor of 5 to 10 (Fig. 4B), whereas the PDGFR TMD fused at the same rate as the native VAMP2 TMD at all numbers of VAMP2s per nanodisc (Fig. 4C). With C18 VAMP2, the fluorescence signal collapsed back to the background level after dithionite injection (fig. S10), which suggests that only the outer leaflets are shared (i.e., hemifusion). By contrast, C45 and PDGFR TMDs achieved full fusion with essentially the same ~50% efficiency as the native VAMP2 TMD. This confirms that a membrane-spanning domain (either lipid or protein) is required to achieve full fusion and also demonstrates that fusion pores open when only the cytosolic domains of the SNARE complex have zippered. Thus, bilayer fusion and the concomitant opening of the nascent pore do not require assembly of the syntaxin and VAMP2 TMDs into the bilayer-spanning helical bundle.

To establish the lifetime of the open pore in these artificial fusion events, we used the calcium release assay. By contrast to lipid mixing, none of the nonnative VAMP2 TMDs efficiently released cargo (Fig. 4, D and E). These experiments show that the native VAMP2 TMD is specifically required for efficient release of vesicle content after the pore opens, which it allows by virtue of lowering the rate of resealing of the nascent fusion pore.

In the nanodisc system, the extent of content release can only be determined by the total amount of time the pore is open before permanently resealing. Should the pore reseal within ~100 μs (as calculated from diffusion constants and vesicle and pore diameter), only a commensurate fraction of the cargo will exit even though the lipids in the disc and vesicle bilayers will have fully mixed. These considerations are fundamental for understanding the different requirements for the number of SNAREs and their TMDs for vesicle fusion and content release, as revealed by our nanodisc experiments. Specifically, our results suggest that although a single SNARE complex suffices to open a fusion pore between nanodisc and vesicle, this pore is too short-lived to allow much transmitter to exit before the pore closes. Only when there are several or more SNAREpins assembling at the same pore does it remain open long enough for effective transmitter release. Even if there are enough SNAREs, it appears that the pore is short-lived unless the TMDs of VAMP2 and syntaxin can zipper in the bilayer to keep the pore open in one way or another, perhaps by pushing outward radially as their TMDs zipper within the bilayer. A single zippering SNAREpin could not do this, which explains why it would necessarily be ineffective. But it is easy to see that three or more SNAREpins pushing away from each other radially could channel the energy of trans-bilayer zippering to keep the nascent pore open. In this speculative model, the restraining force against resealing may only last for as long as it takes the TMDs to zipper. That length of time is likely to be much more than 100 μs, based on the maximum speed for folding of a two-helix coil (*26*–*28*) and considering the higher viscosity of hydrocarbon relative to water (*29*); this would be more than enough time to allow complete neurotransmitter release.

A previous study showing that a single SNARE complex could mediate vesicle-vesicle fusion also measured content mixing (*30*). Interestingly, normalizing the published data for SNARE-free vesicles (see supplementary text and table S1) reveals that here, too, content mixing is greatly reduced relative to bilayer fusion with one SNARE complex per vesicle. Vesicle-vesicle fusion is inherently a poor model of neurotransmitter release through a nascent fusion pore because content mixing occurs not only through a nascent pore (as in nanodiscs and at the synapse) but also subsequently as the vesicles more slowly complete their fusion. Yet despite these limitations, indications of the mechanism we have uncovered can still be found.

These findings provide a simple mechanistic basis for understanding published data that had seemed to be contradictory. Titrations of dominant-interfering SNARE mutants in permeabilized or intact neurosecretory cells suggest a minimum requirement for three SNAREpins to open a fusion pore sufficient for neurotransmitter efflux (*31*, *32*). A quantitative analysis of titrations of botulinum toxin A in relation to cleavage of SNAP25 has been interpreted to mean that a minimum of 10 to 15 SNAP25 molecules are required (*33*), but this analysis assumes that all SNAP25 is present in SNARE complexes and must be considered an upper limit only. By contrast, an elegant single-particle, single-molecule analysis combined with vesicle fusion reactions clearly established that a single SNAREpin was present in many fused vesicles (*30*). We can now see that all of these results emerge from a single underlying mechanism in which the dynamics of the nascent fusion pore are determined by the number of SNAREpins involved. Synaptic vesicles have ~70 copies of the v-SNARE VAMP2 (*6*) and the active zone is rich in t-SNAREs (*34*),

ensuring that multiple SNAREpins are always available to keep the pore open and let transmitter out as rapidly as possible.

References and Notes

1. T. C. Südhof, *Annu. Rev. Neurosci.* **27**, 509 (2004).
2. A. Albillos *et al.*, *Nature* **389**, 509 (1997).
3. L. J. Breckenridge, W. Almers, *Nature* **328**, 814 (1987).
4. D. Bruns, R. Jahn, *Nature* **377**, 62 (1995).
5. Q. Fang *et al.*, *Proc. Natl. Acad. Sci. U.S.A.* **105**, 15388 (2008).
6. S. Takamori *et al.*, *Cell* **127**, 831 (2006).
7. Y. Hu, L. Qu, T. Schikorski, *Synapse* **62**, 953 (2008).
8. T. K. Ritchie *et al.*, *Methods Enzymol.* **464**, 211 (2009).
9. J. Frauenfeld *et al.*, *Nat. Struct. Mol. Biol.* **18**, 614 (2011).
10. H. Katayama *et al.*, *Proc. Natl. Acad. Sci. U.S.A.* **107**, 3453 (2010).
11. K. D. Brewer, W. Li, B. E. Horne, J. Rizo, *Proc. Natl. Acad. Sci. U.S.A.* **108**, 12723 (2011).
12. T. Weber *et al.*, *Cell* **92**, 759 (1998).
13. C. Hu *et al.*, *Science* **300**, 1745 (2003).
14. T. Söllner *et al.*, *Nature* **362**, 318 (1993).
15. R. B. Sutton, D. Fasshauer, R. Jahn, A. T. Brunger, *Nature* **395**, 347 (1998).
16. F. Li *et al.*, *Nat. Struct. Mol. Biol.* **14**, 890 (2007).
17. J. A. McNew *et al.*, *J. Cell Biol.* **150**, 105 (2000).
18. E. A. Smith, J. C. Weisshaar, *Biophys. J.* **100**, 2141 (2011).
19. Y. Xu, F. Zhang, Z. Su, J. A. McNew, Y. K. Shin, *Nat. Struct. Mol. Biol.* **12**, 417 (2005).
20. R. G. Staal, E. V. Mosharov, D. Sulzer, *Nat. Neurosci.* **7**, 341 (2004).
21. E. N. Pothos, V. Davila, D. Sulzer, *J. Neurosci.* **18**, 4106 (1998).
22. R. Khanin, H. Parnas, L. Segel, *Biophys. J.* **67**, 966 (1994).
23. X. Han, C. T. Wang, J. Bai, E. R. Chapman, M. B. Jackson, *Science* **304**, 289 (2004).
24. E. Fdez, M. Martínez-Salvador, M. Beard, P. Woodman, S. Hilfiker, *J. Cell Sci.* **123**, 2473 (2010).
25. A. Stein, G. Weber, M. C. Wahl, R. Jahn, *Nature* **460**, 525 (2009).
26. J. Kubelka, J. Hofrichter, W. A. Eaton, *Curr. Opin. Struct. Biol.* **14**, 76 (2004).
27. W. Y. Yang, M. Gruebele, *Nature* **423**, 193 (2003).
28. K. A. Dill, S. B. Ozkan, T. R. Weikl, J. D. Chodera, V. A. Voelz, *Curr. Opin. Struct. Biol.* **17**, 342 (2007).
29. E. Karatekin, O. Sandre, F. Brochard-Wyart, *Polym. Int.* **52**, 486 (2003).
30. G. van den Bogaart *et al.*, *Nat. Struct. Mol. Biol.* **17**, 358 (2010).
31. Y. Hua, R. H. Scheller, *Proc. Natl. Acad. Sci. U.S.A.* **98**, 8065 (2001).
32. R. Mohrmann, H. de Wit, M. Verhage, E. Neher, J. B. Sørensen, *Science* **330**, 502 (2010).
33. C. Montecucco, G. Schiavo, S. Pantano, *Trends Biochem. Sci.* **30**, 367 (2005).
34. T. Lang *et al.*, *EMBO J.* **20**, 2202 (2001).

Acknowledgments: Supported by Agence Nationale de la Recherche grant 09-Blanc-0129 (F.P.), NIH grants (J.E.R.), and a Partner University Funds exchange grant between the Yale and Ecole Normale Supérieure laboratories. We thank J. Shen (University of Colorado, Boulder) for providing the PDGFR-VAMP2 expressing vector; R. Beck, E. Rhoades, E. Karatekin, and A. Nath for many helpful discussions; and W. Xu and J. Coleman for their kind help.

Supporting Online Material

www.sciencemag.org/cgi/content/full/335/6074/1355/DC1
Materials and Methods
SOM Text
Figs. S1 to S13
Tables S1 and S2
References (*35*–*39*)

7 October 2011; accepted 7 February 2012
10.1126/science.1214984

ER Cargo Properties Specify a Requirement for COPII Coat Rigidity Mediated by Sec13p

Alenka Čopič,* Catherine F. Latham,* Max A. Horlbeck, Jennifer G. D'Arcangelo, Elizabeth A. Miller†

Eukaryotic secretory proteins exit the endoplasmic reticulum (ER) via transport vesicles generated by the essential coat protein complex II (COPII) proteins. The outer coat complex, Sec13-Sec31, forms a scaffold that is thought to enforce curvature. By exploiting yeast bypass-of-sec-thirteen (*bst*) mutants, where Sec13p is dispensable, we probed the relationship between a compromised COPII coat and the cellular context in which it could still function. Genetic and biochemical analyses suggested that Sec13p was required to generate vesicles from membranes that contained asymmetrically distributed cargoes that were likely to confer opposing curvature. Thus, Sec13p may rigidify the COPII cage and increase its membrane-bending capacity; this function could be bypassed when a *bst* mutation renders the membrane more deformable.

Hierarchical assembly of the COPII coat on the cytosolic face of the endoplasmic reticulum (ER) membrane couples cargo selection with membrane deformation to generate functional transport vesicles (*1*). All members of the COPII coat are thought to contribute to generation of membrane curvature (*2*, *3*); however, the precise mechanism of membrane deformation by the COPII coat remains unclear (*4*). We sought to probe this process by dissecting the molecular function of the outer coat complex, composed of Sec13 and Sec31, which is thought to drive membrane curvature by polymerization into a latticelike spherical structure (*3*). Sec13 is unique among COPII proteins in performing multiple functions, driven by structurally analogous interactions with distinct partners, including its canonical partner Sec31 (*5*), the nucleoporin Nup145 (*6*), and the COPII scaffold Sec16 (*7*). Given the pleiotropic functions of Sec13 and the essential nature of COPII-mediated traffic, it is surprising that yeast Sec13p is dispensable in the context of bypass-of-sec-thirteen (*bst*) mutations (*8*, *9*). We sought to exploit this phenotype to probe vesicle formation in the context of a compromised coat complex.

The COPII "cage" self-assembles from rod-shaped Sec13-Sec31 edge elements, four of which come together at vertex regions (*3*). Sec31 is thought to drive assembly: The edge element is formed by stable dimerization at the α-solenoid ancestral coat element (ACE) domain; four edge elements come together at cage vertices via N-terminal β propellers (*5*). Sec13 lies sandwiched between the ACE and β-propeller domains, forming a six-bladed β propeller that is complemented by an additional β blade formed by the domain insertion motif (DIM) of Sec31 (Fig. 1A). We first demonstrated that the essential function of yeast Sec13p was in the COPII coat by restricting its interaction to Sec31p (*10*): An in-frame fusion where Sec13p was inserted immediately downstream of the Sec31p DIM complemented both *sec13*Δ and *sec31*Δ strains, whereas a fusion containing the Sec13p structural homolog, Seh1p, was unable to support viability (Fig. 1B) despite being functional in a *bst*Δ background (fig. S1). Furthermore, uncoupling Sec13p from the COPII coat by mutation of the Sec31p DIM, either by point mutations (*sec31-DK*) or by complete replacement with a 13 amino acid stretch of Gly-Ser repeats ($sec31\text{-}GS_{13}$), failed to support viability except in the context of an additional *bst1*Δ mutation (Fig. 1C), effectively mimicking a *sec13*Δ mutation. We investigated whether Sec31p could engage with the COPII coat independent of Sec13p. Indeed, Sec31p, expressed and purified from insect cells to preclude copurification of Sec13p, was efficiently recruited to synthetic liposomes in the presence of the inner COPII coat, Sar1p-Sec23p-Sec24p (Fig. 1D). Furthermore, the Sec31p DIM mutants also assembled with the inner coat but were unable to recruit Sec13p (Fig. 1D). Finally, we used an in vitro vesicle formation assay (*11*) to confirm that Sec31p was sufficient to generate COPII vesicles in the absence of Sec13p, albeit with reduced efficiency (Fig. 1E).

If Sec31p can generate COPII vesicles on its own, what is the molecular function of Sec13p and what are the in vivo conditions created by the *bst* mutations that permit Sec31p to function in its absence? We used synthetic genetic array technology (*12*) to exhaustively survey the yeast genome for *BST* genes. Two query mutations—$sec31\text{-}GS_{13}$ and *sec13*Δ—were introduced into the yeast deletion collection, and haploid double mutants were scored for viability (Fig. 2A and fig. S2). Three comprehensive screens yielded

Department of Biological Sciences, Columbia University, New York, NY 10027, USA.

*These authors contributed equally to this work.
†To whom correspondence should be addressed. E-mail: em2282@columbia.edu

Supporting Online Material for

SNARE Proteins: One to Fuse and Three to Keep the Nascent Fusion Pore Open

Lei Shi, Qing-Tao Shen, Alexander Kiel, Jing Wang, Hong-Wei Wang, Thomas J. Melia, James E. Rothman,* Frédéric Pincet*

*To whom correspondence should be addressed. E-mail: james.rothman@yale.edu (J.E.R.); pincet@lps.ens.fr (F.P.)

Published 16 March 2012, *Science* **335**, 1355 (2012)
DOI: 10.1126/science.1214984

This PDF file includes:

Materials and Methods

Protein purification

t-SNARE complexes of rat Syntaxin 1A and mouse SNAP25 were expressed and purified with expression vector pTW34 as previously described (35). Full length WT mouse VAMP2 (pet-SUMO-VAMP2) and chimeric VAMP2-PDGFR-TM (pet-SUMO-VAMP2-PDGFRTM, kindly provided by Dr.Jingshi Shen, University of Colorado) were expressed and purified as previously described (36). MSP1E3D1 expression vector (pMSP1E3D1) was purchased from Addgene Inc, and purified as described before (8). After binding to the His-NTA column, MSP proteins were cleaved off by TEV protease overnight at 4°C.

Nanodiscs preparation

Nanodiscs were prepared as described (8). Briefly, the palmitoyl-2-oleoyl phosphatidylcholine (POPC): 1,2-dioleoyl phosphatidylserine (DOPS): N-(7-nitro-2,1,3-benzoxadiazole-4-yl)-1,2-dipalmitoyl phosphatidylethanolamine (NBD-DPPE): N-(Lissamine rhodamine B sulfonyl)-1,2-dipalmitoyl phosphatidylethanolamine (rhodamine-DPPE)=82:15:1.5:1.5(Avanti Polar Lipids) lipid mixture was dried under Nitrogen flow and followed by vacuum for 1 hour. Then the lipid film was suspended in the reconstitution buffer (100 mM NaCl, 20mMTris) with MSP and 6XHis-SUMO-VAMP2 as well as 1% OG. The protein lipid ratio is MSP:lipid=2:120. The amount of VAMP2 depended on the sample. The mixture was vortexed at RT for 15-30 min followed by 3 hours shaking at 4°C. SM-2 bio-beads were added into the mixture which was then shaken overnight to remove the detergent. The next day, the v-discs (with 6XHis-SUMO-tag) were purified with His-NTA beads. VAMP2 free nanodiscs were washed away with reconstitution buffer (containing 20 mM imidazole). The v-discs were eluted with reconstitution buffer containing 400 mM imidazole and then dialyzed overnight. 6XHis-SUMO tags were cleaved off by SUMO protease during the dialysis. Gel filtration was performed to separate the v-disc from 6XHis-SUMO tag and sumo protease. The v-disc sample collections was concentrated by Amicon ultra (0.5ml, 30kDcutoff) centrifugal filter units. To get v-discs with different VAMP2 copies per disc, the different starting MSP:VAMP2 ratio used were, respectively: 2:0.2 (ND1), 2:0.5 (ND2), 2:1 (ND3), 2:2 (ND4), 2:4 (ND5), 2:6 (ND7) and 2:8 (ND9). Correspondingly, same starting MSP:PDGFR-VAMP2 ratios were used to prepare PDGVR-V discs with different chimeric PDGFR-TM-VAMP2 copies per disc respectively.

The CDV-C18-disc or CDV-C45-discs were prepared according to a method described before (22). 1,2-dioleoyl-sn-glycero-3-phosphoethanolamine-N-[4-(p-maleimidophenyl)butyramide] (C18, Avanti Polar Lipids) or C45 was dried and then mixed with cytosolic domain of VAMP2 (CDV) with c-terminal cysteine in disc reconstitution buffer containing 1% OG. The mixture was vortexed for 30 min at RT and then the incubation was continued for another 1 hour standing to allow the coupling of CDVwith C18 (CDV-C18) or C45 (CDV-C45). 5 µl of 100 mM mercapitoethanol was added into the system to stop the reaction. The mixture was purified with His-NTA beads to remove the extra unreacted C18 or C45. The purified product, CDV-C18 or CDV-C45 could be used to prepare CDV-C18 discs or CDV-C45 discs according to the method described above.

Proteoliposomes preparation

Proteoliposomes were prepared as described previously (36). To prepare the t-liposomes with calcium encapsulation, the dry lipid film (1,2-dioleoyl-sn-glycero-3-phosphocholine (DOPC, Avanti Polar Lipids) and t-SNARE proteins were suspended with 400 µl reconstitution buffer: 350 mM KCl, 25 mM Hepes, 50 mM CaCl2 and 1% OG buffer, shaken for 15min at room temperature, and 1ml of 50 mM CaCl2, 25 mM HEPES buffer was added during vortex. The mixture was dialysed with 4 liters of 175 mM KCl, 25mM Hepes buffer overnight at 4°C. The next day, the liposomes were collected and mixed with equal amount of 80% Nycodenz, then loaded into the bottom of Beckman ultra-clear centrifuge tube (11x60 mm). 500 µl of 30% and 20% Nycodenz were laid over the sample and then 250 µl dialysis buffer on the top. After 3 hour 40 minutes of ultracentrifuge at 50,000 rpm, samples were collected between 0/20% Nycodenz interface (2x200 µl). The liposomes loading with EDTA or EGTA were prepared similarly with the reconstitution buffer: 400 mM KCl, 25 mM Hepes, 30 mM EDTA or EGTA.

Lipid mixing assays

Lipid mixing assays were performed as standard liposome lipid mixing assays described previously (36). The fusion assay of 50 µl t-liposomes (0.075 µM) and 2.5 µl v-discs (1.5 µM) were performed in 96-well Nunc white plate at 37°C, the liposomes to discs ratio is about 1:1, and NBD signal was monitored by Spectramax M5 microplate reader. After 40 minutes fusion, 10 µl 5% dodecyl-maltoside was added into the fusion system, data were collected for another 20 min to get the maximum NBD signal. The raw NBD-fluorescence data were converted into the percentage of the maximum NBD signal changes.

Dithionite assay

After 40 min fusion reaction, 2.5 µl of 100 mM dithionite (final concentration is 5 mM) were added into the mixture and data were collected for another 20 min until the signal is stable. To completely quench NBD signal, 10 µl 5% of dodecyl-maltoside (detergent) was first added into the fusion system after 40 minutes of reaction to break liposomes then dithionite was used to quench all NBD signal.

Electron microscopy

The nanodiscs or liposomes-nanodiscs samples were applied to a glow-discharged carbon-coated EM grid and negatively stained with 2% uranyl acetate (w/v) solution. The specimen was subsequently examined in an FEI Tecnai-12 electron microscope operated at 120 kV. Micrographs of the specimen were taken on a Gatan Ultrascan4000 CCD camera at a magnification of 52,000. To form the SNARE complexes on v-disc, soluble Syntaxin1A H3 domain and SNAP25N/C domains were co-incubated with v-disc at 4°C overnight and separated by gel filtration to remove the free proteins. Then the samples were applied to the electron microscope as described above.

TIRF imaging

For the acquisition of the TIRF movies a Nikon Ti Eclipse microscope was used. It features laser excitation at 488, 532 and 647 nm. Fluorescence images are collected by a

Nikon 60x/1.45 oil objective and projected onto an EM-CCD camera (Andor iXon DU897E, 512x512 pixels). The filters sets used for Lissamine-Rhodamine were zet532/10x, zt532rdc, HHQ545lp, ET605/70m: and for Alexa647: zet640/20, zt640rdc, HQ660lp and ET 700/75m from Chroma Technology Corp., Rockingham,VT.
The TIRF-microscope was used to monitor the fluorescence bleaching steps of single nanodisc that contained Rho/NBD tagged phospholipid and Alexa647 tagged SNAP25N (K76C). An 8-well chambered cover slide was cleaned by filling 350 µL 0.1 M HF into each chamber and incubation for 2 min. Then the chambers were cleaned each 5x with 350 µL water and 2x with 350 µL buffer. The nanodisc constructs adsorbed to the glass surface once in contact. To prepare nanodisc samples with SNARE complexes for TIRF imaging, v-discs were co-incubated with extra amount (5 times more) of soluble SyntaxinH3 domain and SNAP-25 N(Alexa647 tagged)/C domain overnight at room temperature to form the SNARE complex. Then the disc samples were isolated by gel filtration (Superdex200) to remove the free t-SNARE proteins. The v-nanodisc labeled with cytosolic t-SNARE were diluted to 1 pM and 50-200 uL were added stepwise to the chambers containing 350 uL buffer until the desired density of 200 spots per field of view (0.025/sq-micron) was derived. Movies were taken exiting with 647 nm with a sampling rate of 9.7 Hz (100 ms integration time) after acquisition of the movie a single image was taken with excitation at 532 nm to control the co-localization of nanodiscs and protein. Intensity traces from colocalized spots were extracted from the movies and the number of t-SNAREs was estimated from the bleaching steps and intensity levels observed using ImageJ.

Liposome floatation assay

Liposomes floatation assay was carried out as previously described (36). t-liposomes were incubated with v-discs with or without pre-incubation of CDV at 37°C for 2 hours, then the fusion products were mixed with equal volume of 80% Nycodenz (w/v) in reconstitution buffer to get 40% Nycodenz mixtures. The 40% Nycodenz mixture was transferred to 5 x 41 mm centrifuge tubes and overlaid with 200 µl each of 30% and 20% Nycodenz and then with 20 µl reconstitution buffer on the top. Centrifugation was performed at 48,000 rpm for 4 hours. Samples were collected from the 0/30% Nycodenz interface (2 x 20 µl) and 40% Nycodenz layer and then analyzed by western blot with MSP antibody.

Toxin assay

The v disc alone or float-up products of t-liposome and v-disc mixture (incubated at 37°C for 2 hours) were incubated with BoNT or TeNT with 100 µM Zn2+ at 37°C for 2 hours, then protein sample were analyzed by SDS PAGE-Coomassie blue stain.

Content release assay

To monitor the lipid mixing and content release, two fusion reactions were set up in parallel: to monitor the lipid mixing, 50 µl t-liposomes with cargoes as indicated above were mixed with 2.5 µl v-discs and then loaded into a 96 well plate. NBD signal was collected by Spectramax M5 microplate reader set at ex/em: 460nm/538nm, cutoff 530nm. To monitor the calcium release, exact same gradients as well as 2 µM mag-fluo-4 (final concentration) were mixed and mag-fluo-4 signal was recorded by plate reader set

at: ex/em:480nm/520nm, cutoff 515nm. After 40 minutes fusion, 10 µl 5% dodecyl-maltoside was added into the fusion system, data were continued to collect for another 20 min to get the maximum mag-fluo4 signal. The relation between mag-fluo4 signal and calcium concentration was independently established. The data are plotted as the percentage of total calcium released with time. The EDTA or EGTA release assays were performed similarly with t-liposomes loading with EDTA or EGTA. Fluo4 (Kd with calcium: 345 nM) was used as calcium indicator.

SOM Text

Calculation of the fraction of full fusion events

Two types of dithionite experiments were performed (see supplementary figure S4, bottom). First, dithionite was directly added at the end of the fusion assay. This directly provided the fluorescence due to the protected NBD. Second, detergent was added at the end of the fusion assay. Dithionite was subsequently injected in the sample. This approach quenches all the NBD dyes and provided the background fluorescence F_{bk}. The fluorescence obtained after addition of dithionite (no detergent), F_{dith}, comes from the protected NBD. So, the total fluorescence from these protected lipids is: $F_{dith} - F_{bk}$. The total fluorescence in the system is measured in presence of detergent before addition of dithionite and is equal to: $F_{det} - F_{bk}$. Hence, the fraction of nanodiscs that have been through a full fusion event, f_{full}, is then expressed as:$f_{full} = \frac{2(F_{dith} - F_{bk})}{F_{det} - F_{bk}}$. The prefactor "2" is because only half of the lipids from a fully fused nanodic are on the interior leaflet of the liposome.

At the beginning of the fusion assay, the fluorescence, F_{init}, comes solely from the nanodiscs. Thus, the contribution of the nanodiscs to the fluorescence is: $F_{init} - F_{bk}$. The maximum fluorescence during the fusion assay, F_{max}, is the sum of the contribution of the unreacted nanodiscs, the fused nanodiscs and the nanodiscs that shared a side with the outer layer of a liposome ("hemifused"). The fraction of the latter, f_{hemi}, can be directly expressed as:

$$f_{hemi} = \frac{2\left((F_{max} - F_{bk}) - f_{full}(F_{det} - F_{init}) - (F_{init} - F_{bk})\right)}{(F_{det} - F_{init})}$$

Then, $1 - f_{full} - f_{hemi}$ represents the fraction of unreacted nanodiscs. Hence, the fraction of fusion events that corresponds to full fusion is $f_{full}/(f_{full} + f_{hemi})$.

Estimate of the pore size

In the liposome, one solute molecule collides with the membrane at a frequency $\boldsymbol{\vartheta_0}$. The probability that one collision is within the effective surface where the solute can pass through the pore is $\frac{(r_p - r_s)^2}{4R^2}$. Where $\boldsymbol{r_p}$, $\boldsymbol{R}$ and $\boldsymbol{r_s}$ are respectively the pore radius, the liposome radius and the Stokes radius of the solute molecule. Hence the characteristic time for solute release is $\frac{4R^2}{\vartheta_0(r_p - r_s)^2}$.

Knowing that the release of EDTA is 2.3 times faster than that of EGTA, it is possible to determine the pore size. Using the Wilke-Chang correlation for the diffusion coefficient

of the solute (37), the Stokes radius is given by $\frac{V^{0.6}k_B}{44.4.10^{-8}\pi(2.6M)^{0.5}}$ where k_B is Boltzman's constant, M the molecular weight of the solvent in $g.mol^{-1}$ and V the molar volume of the solute $cm^3.mol^{-1}$. V is calculated using the Schroder increments (37). For EDTA and EGTA, this leads to ~0.4 nm and ~0.5 nm Stokes radii respectively.
Since the ratio between the EDTA and EGTA characteristic times is 2.3, the pore radius can be roughly estimated by:

$\frac{(r_p-0.4)^2}{(r_p-0.5)^2} = 2.3$, i.e, r_p =0.7 nm, corresponding to a ~1.5 nm pore. The relative dimensions of the liposome, the nanodisc and the pore are indicated in Fig. S11.

A minimum of ~3 SNAREpins are required for fast and efficient release

All wild-type VAMP2 and PDGFR-VAMP2 discs display the same kinetics for bilayer fusion with t-liposomes. The content release after 40 minutes incubation in our experiments is presented in Fig. S12A. For VAMP2, there is a notable increase of calcium release beyond ND2 followed by a plateau beyond ND7. For all PDGF-VAMP2 samples, the release remains low (3-4%) and does not vary significantly with copy number. At low wild-type VAMP2 copy numbers (ND1 and ND2) and for all PDGFR-VAMP2 samples the pore is too short-lived and too small to permit full content release. By contrast, when more wild-type VAMP2 are present, the plateau attests that maximum release can be achieved when a sufficient number of SNAREpins are engaged in the fusion process. The inflection point in the maximum calcium release is located close to 5 VAMP2 per nanodisc on average. Since VAMP2 will be distributed between both sides of the disc, one face of the nanodisc will have typically 3 VAMP2. To try to quantitatively model this observation, we have assumed, as suggested by our step-bleaching experiments (Fig. S13) and by previous observations on liposomes (38, 30), that the VAMP2 are randomly distributed within each nanodiscs sample, meaning they follow a Poisson distribution. Assuming a random distribution between the two sides of each disc, it is possible to determine the total distribution of VAMP2 among the nanodisc faces for each sample (Fig. S12B). The calcium release fits a "cooperative" model where there is a limited release when one SNAREpin is engaged and a sudden increase in content release above a threshold when enough SNAREpins are involved (Fig S12C). From this model, the threshold number of SNAREpins for efficient content release is ~ 3, which is consistent with in vivo observations.

Comparison with the results in van der Bogaart et al.(30)

A recent study by van den Bogaart et al. (30), also showed that a single SNARE complex could mediate vesicle-vesicle fusion. They also measured content mixing that seemed to be correlated to lipid mixing when reducing SNARE density. The apparent difference between these results and ours is due to the fact that, in this other work, they have a significant number of liposomes without any SNARE in their assay. These liposomes will not be able to fuse which leads to an apparently much lower fusion rate. By contrast, in our assay, we remove any nanodisc not containing v-SNAREs.

In the results of van den Bogaart et al., once the fusion rate is normalized by the number of liposomes having t-SNAREs, there is no change in the lipid mixing between liposomes whether they have 1 SNAREs or 20 SNAREs (see Table S1 below and Fig. 4a

of van den Bogaart et al.). Thus, just like us, they observe the same fusion rate at all SNARE concentrations.

Regarding the content release, van den Bogaart et al. could not restrain the fusion pore. Hence, some of the content may be released during the expansion phase. So, we would expect the release to be the same with 1 or 20 SNAREs. However, they observe a decrease of content release which indicates that, in some cases, the pore did not expand and resealed just as we observe in our assay.

Hence, despite the vesicle-vesicle fusion assay, indications of the mechanism we have uncovered with pores constrained against expansion are still evident. This suggests the underlying properties we have found with discs apply to vesicles also.

Fig. S1 Docking is rate-limiting in the ND-liposome fusion assay

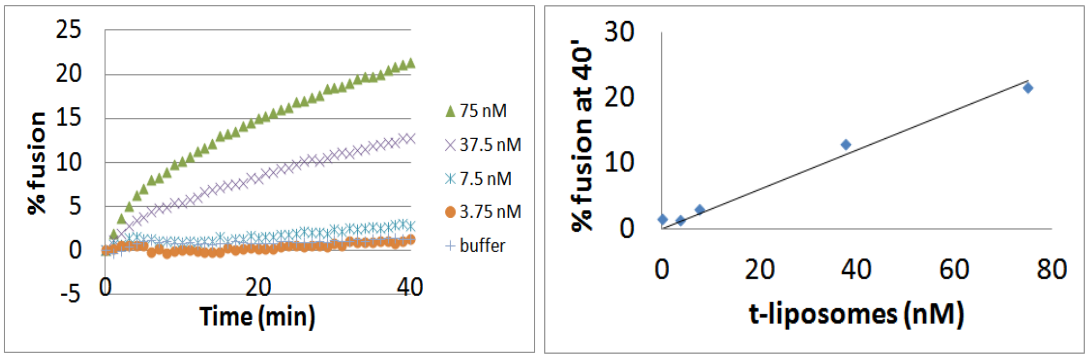

Lipid mixing experiments were performed with ND1 at various t-liposome concentrations (left). The total fusion after 40 minutes is displayed on the right. Because we used ND1, t-SNAREs were always in excess compared to v-SNAREs.
Either docking or fusion is limiting in this experiment. If fusion is limiting, v-discs should quickly dock independently of the t-liposome concentration and the total fusion rate should remain constant. If docking is limiting, the probability of a v-disc to dock will vary linearly with the t-liposome concentration and fusion will occur immediately. Hence, the fusion rate will vary linearly with the liposome concentration. Since a linear dependency is observed here (right), docking is the limiting step in our assay.

Fig. S2 t-NDs fuse with v-liposomes.

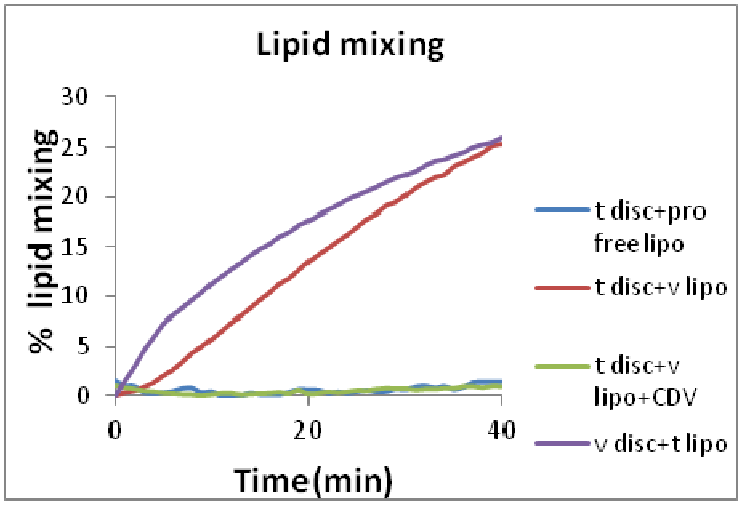

The graph shows the comparison of the lipid mixing assay for t-discs vs v-liposomes and v-disc vs t-liposomes. The slight decrease at the start of the t-discs vs v-liposomes curve is due to temperature that was not equilibrated at the start of the experiment. The controls are all performed with t-discs.

Fig. S3: Release of EDTA and EGTA

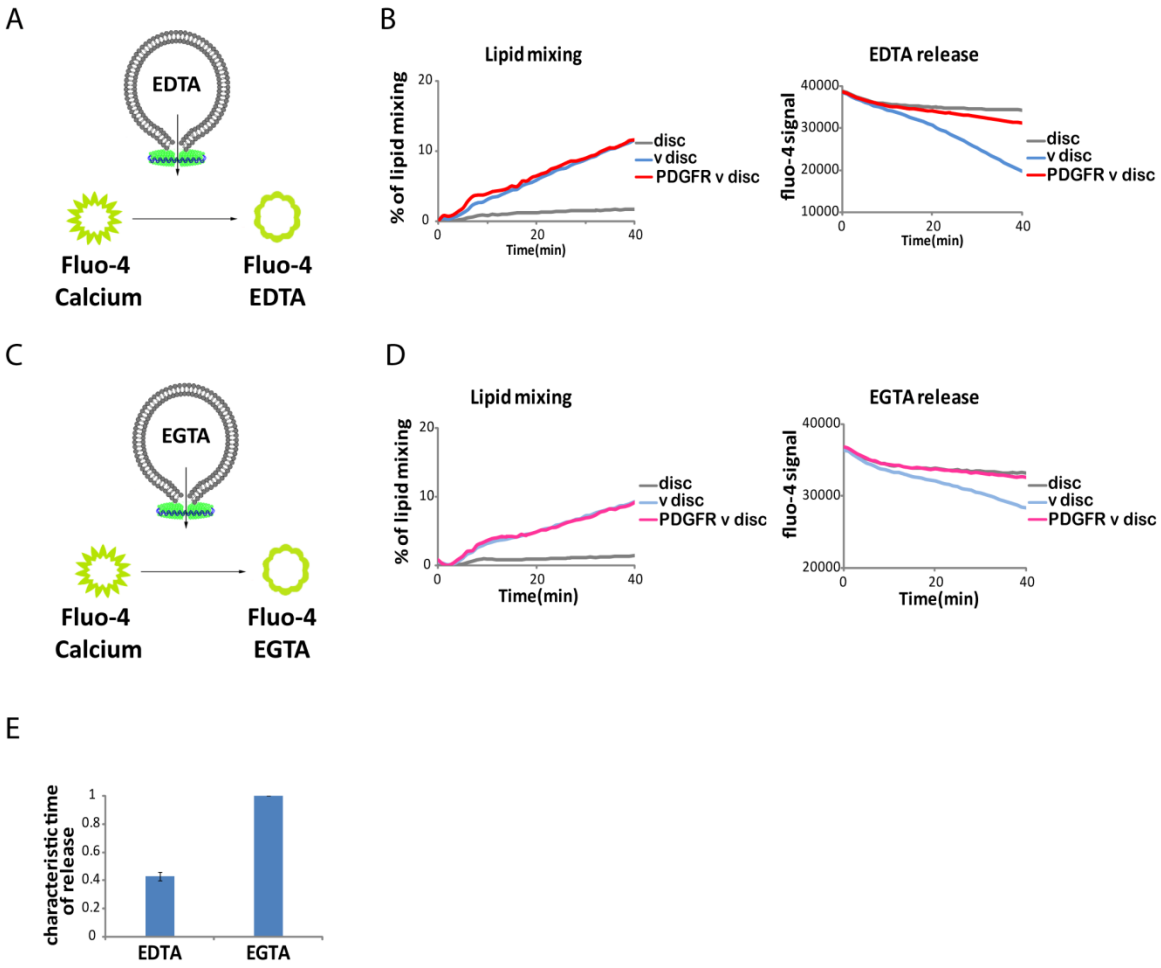

(A) EDTA release assay. 30 mM EDTA is loaded into t-liposomes that fuse with v-discs. 2μM Fluo-4 (with about 15 μM free calcium) is added into the fusion system. During the fusion, EDTA is released from the liposome into the exterior buffer, the Fluo-4 signal decreases as EDTA chelates the calcium in the buffer.
(B) Lipid mixing and EDTA release assay. During the fusion, EDTA is released from liposomes into the exterior buffer. The chimeric PDGFR-VAMP2 displays slower EDTA release kinetics than the wild-type VAMP2.
(C) EGTA release assay. 30mM EGTA is loaded into t-liposomes that fuse with v-discs. System setup is the same as EDTA release assay.
(D) Lipid mixing and EGTA release assay. During the fusion EGTA is released from liposomes into the exterior buffer. The chimeric PDGFR-VAMP2 displays slower EGTA release kinetics than the wild-type VAMP2.
(E) characteristic time of EDTA release is about 2.3 folds faster than that of EGTA release in the fusion. As EDTA and EGTA have similar Ka with calcium (39), we estimate the pore size is about 2 nm by a diffusion model.

Fig. S4: All ND samples display the same protection to dithionite after reacting with t-liposomes

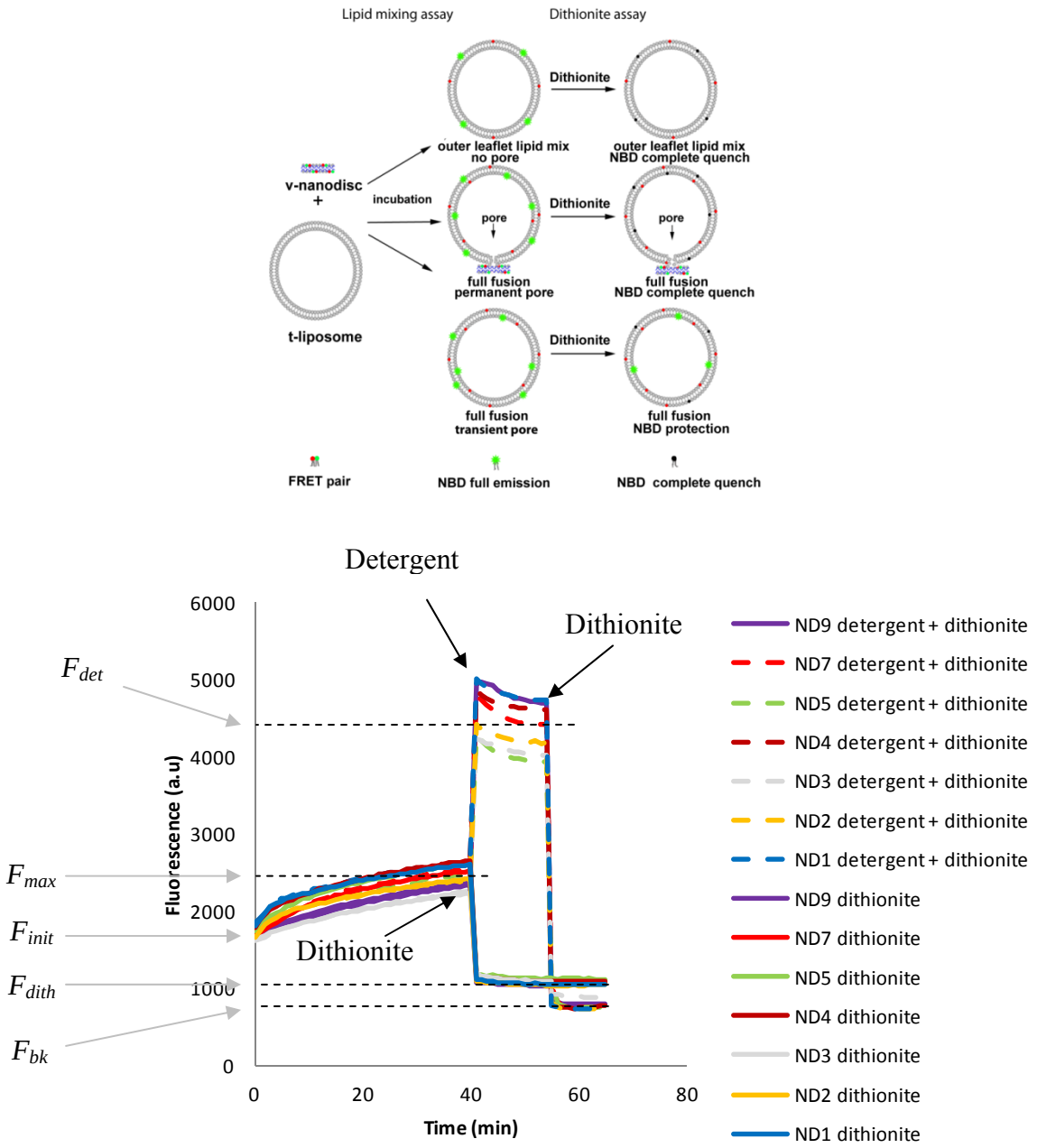

Top: Schematics showing lipid mixing assay and dithionite assay. Lipid mixing assay: v-discs are labeled with NBD-PE and Rho-PE, NBD (green dots) is quenched by Rhodamine (red dots). During the fusion, the fluorescent probes are diluted and NBD signal is enhanced. Three scenarios can happen: (1) hemifusion, (2) full fusion with permanent pore or (3) full fusion with a pore that resealed. Dithionite assay: 5mM dithionite was added into the fusion system after 40 minutes of reaction. Dithionite completely quenches NBD (black dot) in the first two hypothetical conditions. In the last condition, NBD on the inner leaflet of liposome is protected from dithionite.

Bottom: Representative examples of dithionite experiments of the dithionite assay for all the native v-discs samples used. All samples closely overlap and lead to similar fraction of full fusion events (see supplementary text). After 40 minutes of incubation of v-discs with t-liposomes (full lines), dithionite (5 mM) is introduced into the samples to evaluate the amount of protected dye. In the control (dashed lines) samples, detergent was added after 40' followed by dithionite 15' later. The difference between the final fluorescence in the experiment (F_{dith}) and the background signal obtained in the control experiment (F_{bk}) is a direct proof that some fluorophores remain protected. F_{init} is is the initial fluorescence, F_{max} the maximum fluorescence signal reached during the lipid mixing assay and F_{det} the fluorescence signal after detergent was added.

Fig. S5: No pore remains open (control by dithionite)

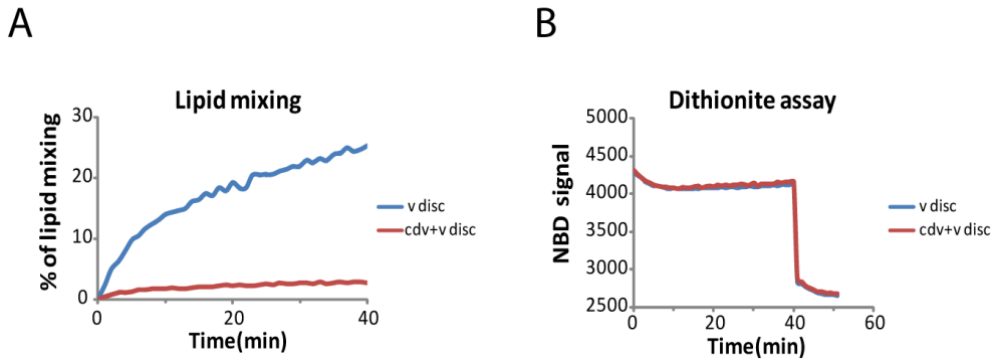

(A) Lipid mixing assay of t-NBD-liposome (0.03%NBD-PE) fusing with v-disc (8%rhodamine-PE). Rhodamine is self-quenched at such high concentration, when v-discs fuse with t-liposomes, Rhodamine fluorescence is increased because of lipid dilution. The percentage of lipid mixing is calculated by the same equation of standard NBD/Rho lipid mixing assay.
(B) Dithionite assay was performed by adding 5mM dithionite after 40 minutes of fusion reaction. Dithionite quenched all the NBD on the outer leaflet of t-liposomes, as well as the NBD on the inner leaflet of t-liposomes if the fusion pore remains open. Otherwise, the NBD on the inner leaflet was protected. The quenches of NBD signal by dithionite were same under the fusion condition (v-discs fusing with t-liposomes) or non-fusion condition (CDV to block v-discs fusion with t liposome), which suggests there were no long-lived fusion pores after v-discs fused with t liposomes.

Fig. S6: The nanodiscs remain attached to the liposomes and the SNAREs are toxin resistant

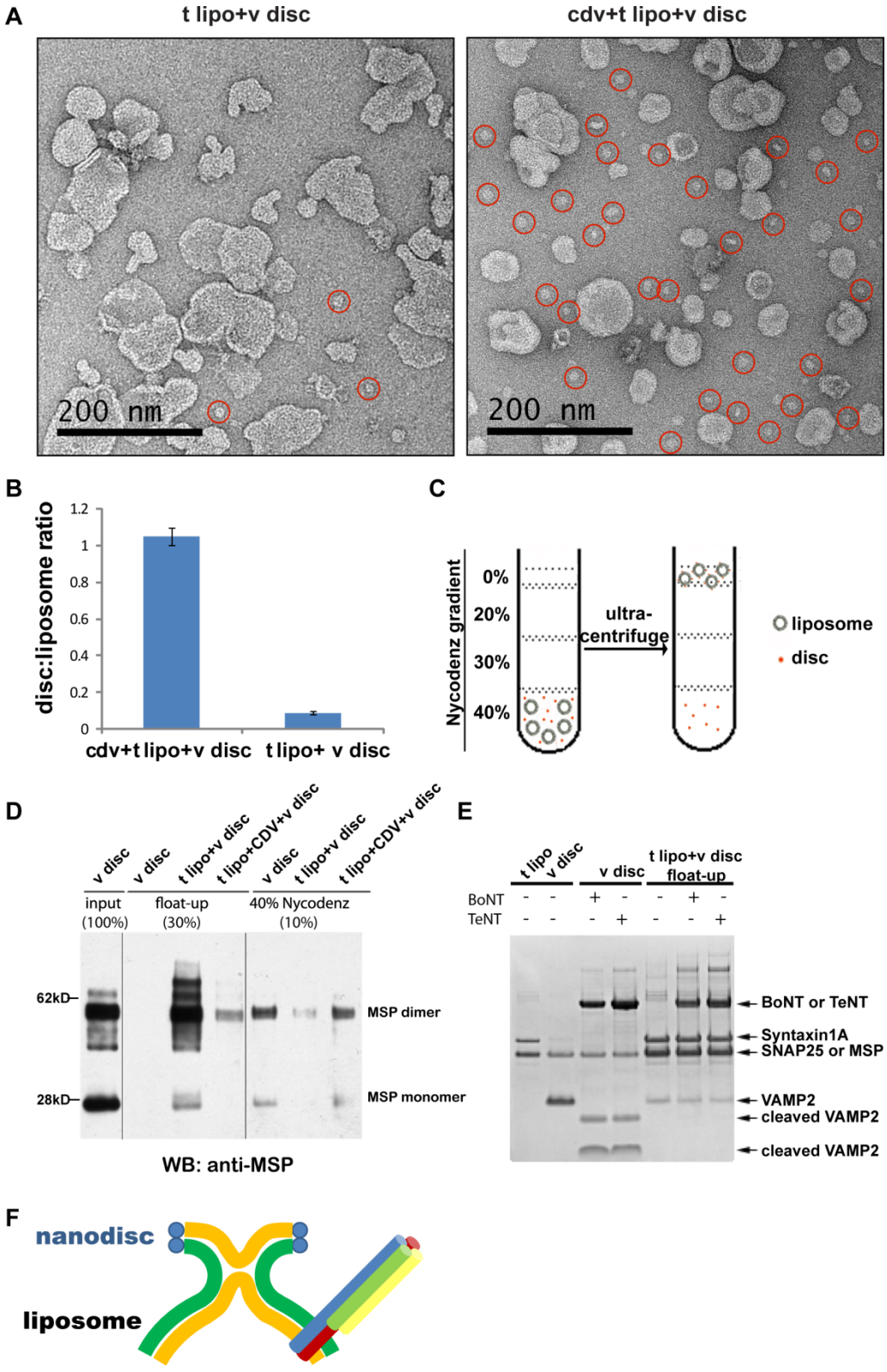

(A) EM images showing the post-fusion products of t- liposomes and v-discs. After fusion, free v-discs (marked with red circles) can hardly be seen, while, when CDV is used to block the fusion, a lot of free v-discs (marked with red circles) can be easily observed under EM.
(B) Statistics of the v-discs:liposomes ratio in Fig. S3A. The ratios were determined in 20 random fields.
(C) Schematics of the liposome floatation assay. Liposomes (with nanodiscs) samples were mixed with equal amount of 80% Nycodenz solution to get the 40% Nycodenz concentration. Then the mixture was transferred into centrifuge tube and overlaid with 30%, 20% Nycodenz solution as well as reconstitution buffer (0% Nycodenz) on the top. Ultra-centrifugation was performed at 48,000 rpm for 4 hours at 4°C. The 40% Nycodenz layer and interface between 20%-0% layers were collected for further analysis.
(D) Western blot analysis of the samples after ultracentrifugation by using anti-apoA1 antibody (Santa Cruz). v-discs per se stay at 40% Nycodenz layer because of their high density. After fusion with t-liposomes, more than 90% MSP appeared in the fraction from 20%-0% interface, which suggests that v-discs bind to and co-float up with liposome. With CDV blockage of fusion, 90% MSP are found in 40% Nycodenz layer, less then 10% MSP occurred in 20%-0% interface fraction. This small remaining binding may due to incomplete blockage of fusion by CDV.
(E) Toxin assay after fusion. VAMP2 is protected from BoNT or TeNT cleavage, which suggests SNAREs may be in cis-conformation. The liposome samples from floatation assay were treated with either BoNT or TeNT at 37°C for 2 hours and then analyzed by SDS-PAGE. Both BoNT and TeNT completely cleaved VAMP2 on v disc. While after fusion of v-discs and t-liposomes, VAMP2 floated-up with t-liposomes, which is consistent with the previous result from MSP Western blot, and no cleavage of VAMP2 by BoNT or TeNT was observed.
(F) The characterization presented in the previous panels of this figure is consistent with the idea that resealing from full fusion is to a hemi-fusion like state in which a stalk of lipid bilayer permanently connects the outer leaflet of the vesicle to what had been the SNARE complex containing leaflet of the nanodisc with cis – SNARE complexes presumably in the liposomes. This is what is presented in this diagram.

Fig. S7 Quantification of the number of VAMP2 and MSP per ND by western blot.

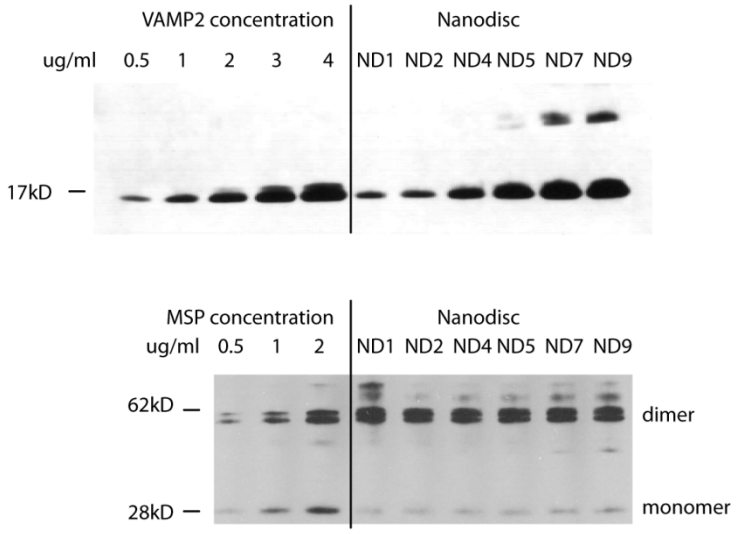

To further determine the number of MSP or VAMP2 per nanodisc, we performed quantitative western blot. As show above, different concentration of VAMP2 (top left panel) or MSP (bottom left panel) proteins were used as the standard, the concentration of VAMP2 or MSP from different v discs were then determined by the integrated density of each blot band by Image J program. Then the number of VAMP2 or MSP per disc was obtained by the ratio of MSP concentration/disc concentration or VAMP2 concentration/disc concentration.

The nanodisc concentration is about 1.5 μM (normalized by NBD fluorescence) and the calculated MSP per nanodisc is about 1.85, consistent with the theoretic number of 2 MSP per disc. The calculated VAMP2 per nanodisc is: ND1(1.2), ND2(2.2), ND4(4.3), ND5(5.5), ND7(7.4), ND9(9.3), which are similar to the ones calculated by Coomassie blue staining method.

Fig. S8 Fraction of full fusion events

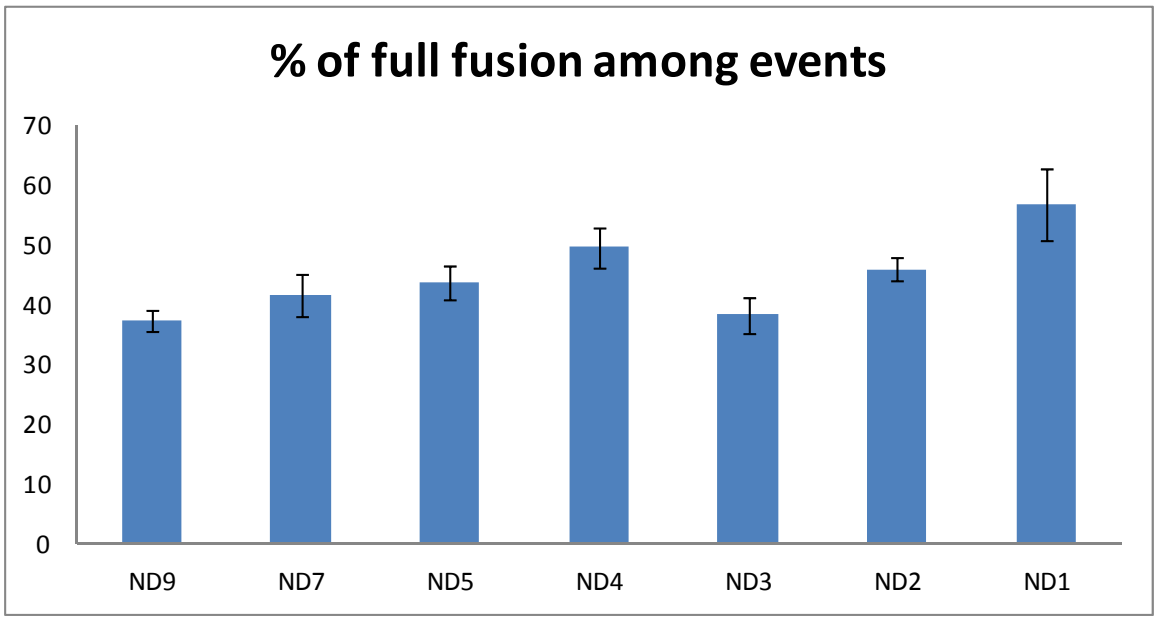

The fraction of full fusion events are calculated according to the method presented in the supplementary text above. For all samples, ~50% of the fusion events correspond to full fusion.

Fig. S9: gel filtration and SDS PAGE with chimeric VAMP2s.

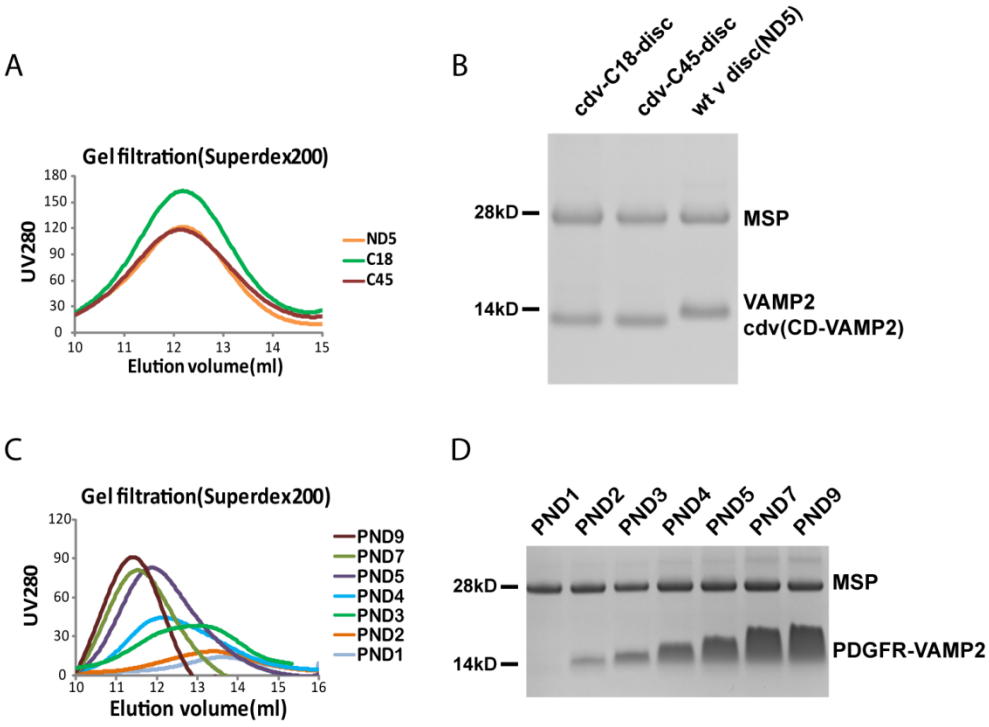

(A) Elution profile of wild type v-discs (ND5), CDV-C18 discs and CDV-C45 discs on Superdex 200 column. Same elution volume suggested these 3 v-disc populations have similar copies of VAMP2 per disc.
(B) SDS-PAGE analysis showing the v-disc samples from Fig. S5A has similar amount of MSP and VAMP2 proteins.
(C) Elution profile of PDGFR-v-discs with different copies VAMP2 per disc. With more VAMP2 incorporation, PDGFR-v-discs showed earlier elution volumes on Superdex200 column.
(D) The PDGFR-v-disc samples obtained by gel filtration were then analyzed by SDS-PAGE gel staining with Coomassie Brilliant Blue.

Fig. S10: Dithionite assay with C18

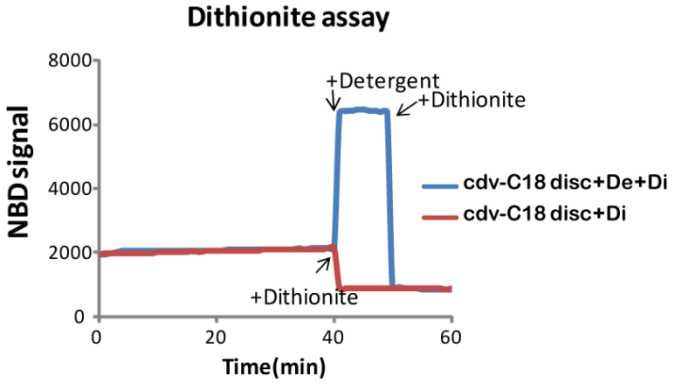

The dithionite assay shows that the fusion of CDV-C18-discs with t-liposomes was solely outer leaflet mixing. After 40 minutes of the fusion of t-liposomes and CDV-C18-discs, dithionite (Di) was added into the reaction to quench NBD signal (red). NBD signal goes down to the same level as control experiment (blue curve) in which detergent (De) and then dithionite were added into the same fusion reaction to completely quench all NBD signal.

Fig. S11 Dimensions involved in the nanodisc/liposome setup

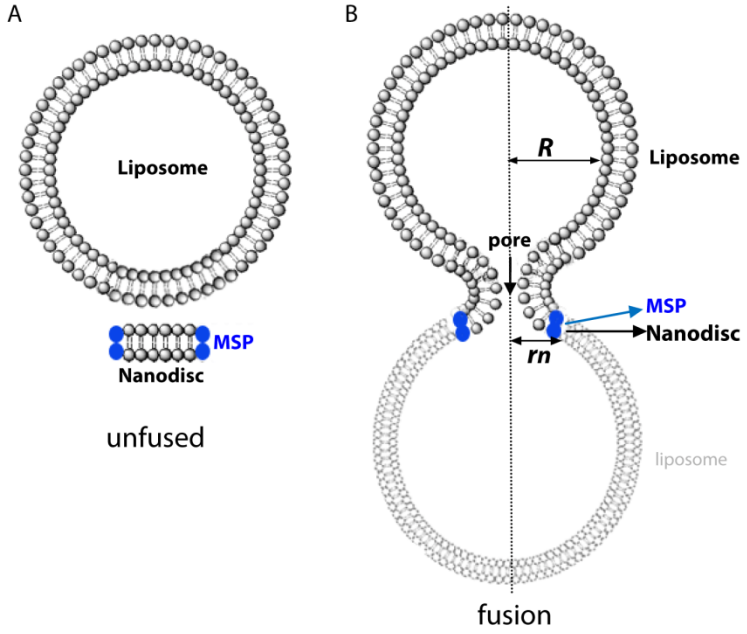

The nanodisc-liposome fusion system
(A) A liposome (diameter: ~50 nm) interacts with a nanodisc (diameter: ~16 nm).
(B) When the liposome fuses with the nanodisc a fusion pore opens (diameter: ~2 nm). Because of the geometrical constraints due to the size of the nanodiscs and the bending modulus of the lipid bilayer, the pore cannot expand. As a reference, liposome-liposome fusion, in which the pore can expand, is indicated with gray liposome at the bottom.

Fig. S12: At least 3 SNAREs are required for fast and efficient release

A. Maximum calcium release

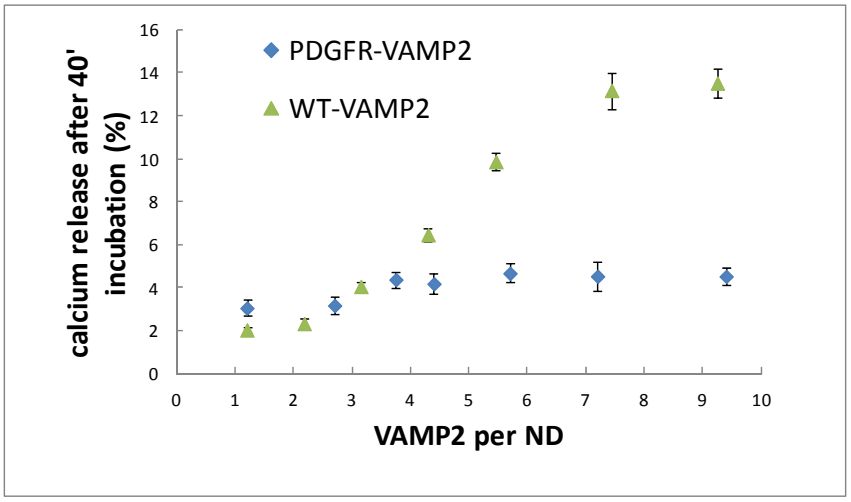

B: Distribution of VAMP2.

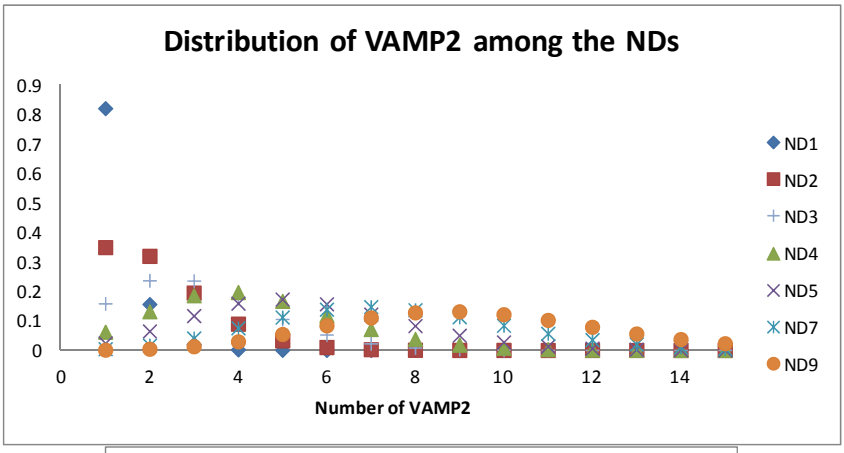

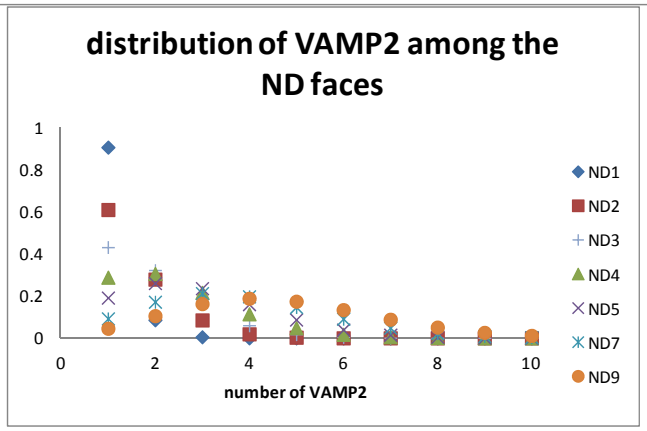

C. Degree of cooperativity

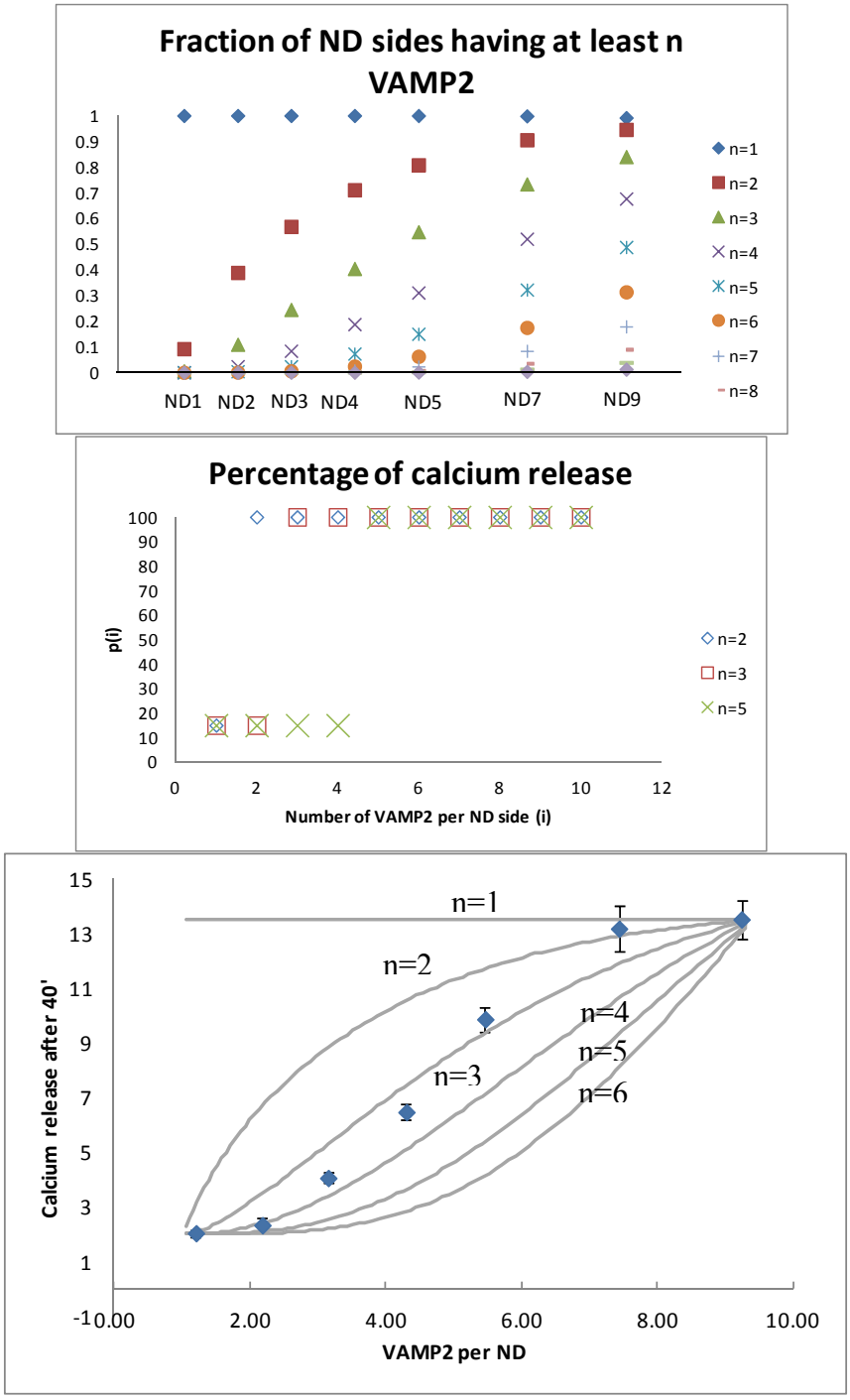

(A) Percentage of calcium released after 40' incubation (End points in Fig. 3D and Fig. 4F). During a fusion event, the calcium release will depend on the number of VAMP2 in the ND side involved. The fraction f(i) of ND sides having i VAMP2 will release on average a percentage p(i) of their calcium content. The total fraction of calcium released is therefore: $\sum_{i=1}^{\infty} f(i)p(i)$. This total release is experimentally obtained. Hence, to estimate p(i), we must first determine f(i).

(B) The number of VAMP2 among the NDs is not homogeneous within each sample but follows a random distribution: a Poisson distribution is expected. Once the protein-free NDs have been removed, the distribution of VAMP2 among the various samples is given by the upper chart. The distribution of VAMP2 among the sides having at least one protein (i.e. able to fuse) is given in the lower chart (assuming VAMP2 distributes randomly between the two sides of each disc). This distribution indicates that f(1) and f(2) can be very well estimated from ND1 and ND2: p(1)~p(2)~15%. From the other samples, it appears that p(i) is larger for i>2. The release being quite linear between ND2 and ND7, we have to find a set of p(i) that provides a linear shape and the right total percentage of calcium release. We envisioned two models: i. The SNAREpins act sequentially and independently and ii. The SNAREpins contributions are cooperative and are more than the sum of each independent one.

(C) Degree of cooperativity. The upper chart indicates the fraction of ND sides having more than n VAMP2 for n=1… 10. Since these variations are almost linear, it is tempting to make the simple assumptions: i. 100% of the vesicle cargo is released when more than n SNAREpins from one ND face are engaged; ii. ~15% of the vesicle cargo is released when less than n SNAREpins from one ND face are engaged (to be consistent with f(1) and f(2)). The average release per full fusion event can be estimated for different n. The experimental data are superimposed to these predictions and seem to agree with n~3.

Fig. S13: Quantification of the VAMP2 distribution in nanodiscs

A. Movie and trace acquisition

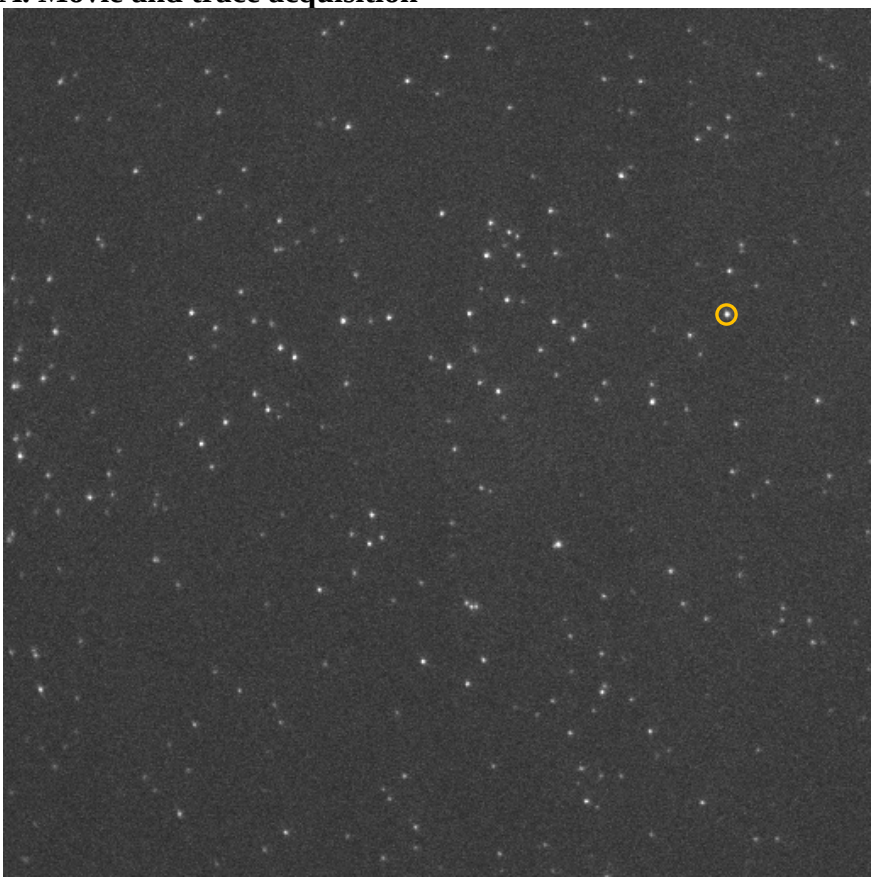

B. Step bleaching traces.

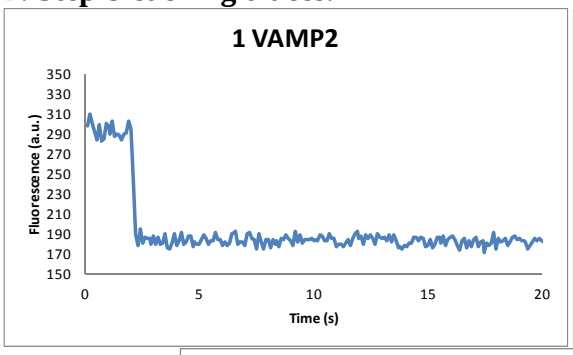

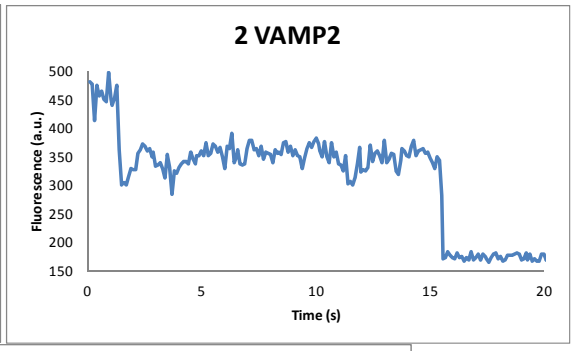

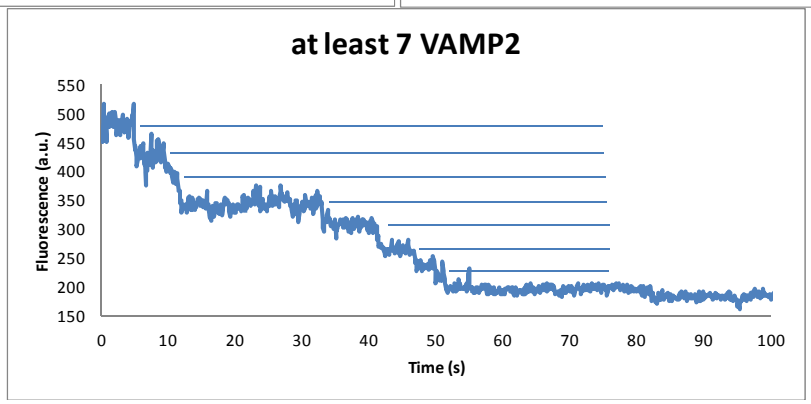

C. Measured VAMP2 distributions

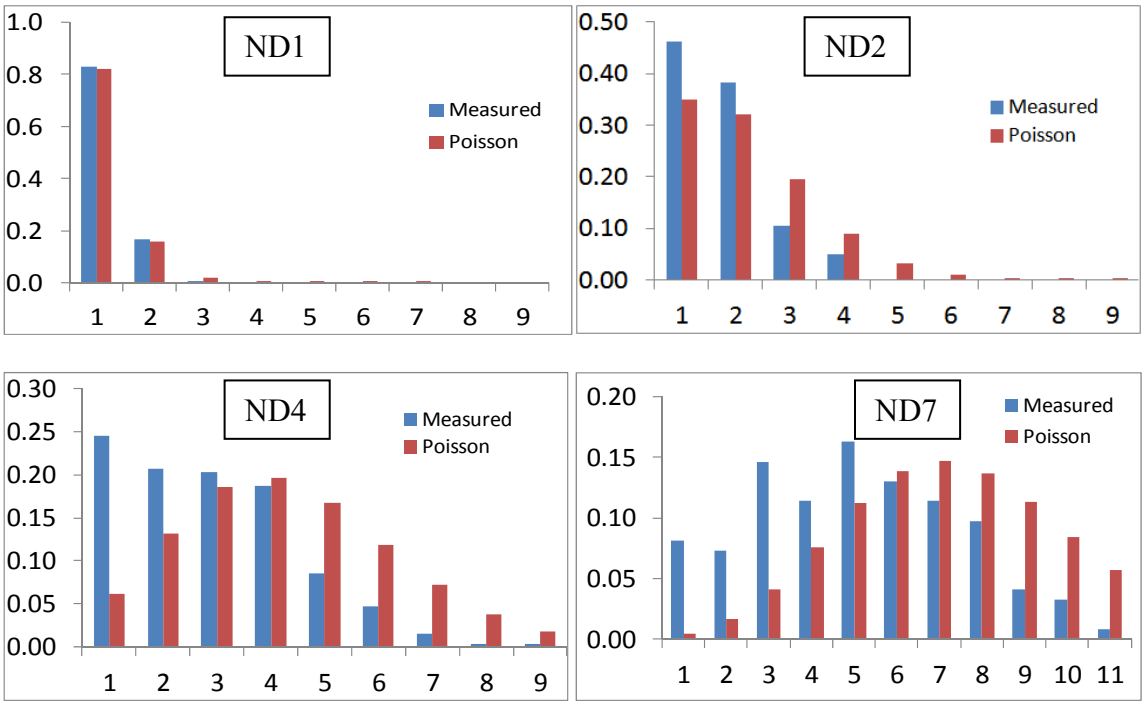

(A) Movies were acquired as described in the supplementary text for four samples, ND1, ND2, ND4 and ND7. In each the average intensity of pixels inside a circle that surrounds one nanodisc is plotted of the whole movie (2-3 minutes at 10 Hz acquisition rate); the orange circle is typical of the circle size that was used. The resulting trace is analyzed for each nanodisc of the field. For each sample, between 120 and 250 nanodiscs from at least two fields were analyzed.

(B) Examples of traces. On top, traces of nanodiscs containing one (left) and two (right) VAMP2. At the bottom, a trace taken from a movie of the ND7 sample shows the complexity to accurately estimate the values when multipleVAMP2 are present. This is due to the mutual quenching of the probes (at high density on the nanodiscs) which lowers the extent of the steps and to the superimposition of many steps. In this case, 7 steps were counted but it is possible more VAMP2 are actually present in the nanodiscs.

(C) The measured VAMP2 distributions for ND1 and ND2 is close to the one expected for a random Poisson distribution (top). For these two samples the average number of VAMP2 is very close to the ones measured by Coomassie blue and Western blot (see table S2). The distributions measured for ND4 and ND7 displays a slightly lower number of VAMP2 than predicted by a Poisson distribution. Similarly, the average numbers of VAMP2 are slightly lower than the ones obtained in Coomassie blue and Western blot. This is due to the difficulty to analyze nanodiscs containing multiple VAMP2: the actual number is underestimated. Hence, the distributions obtained from step bleaching suggest that (i) the average numbers of VAMP2 measured by Coomassie blue and Western blot are correct and (ii) the actual distribution of VAMP2 among the nanodiscs is close to the random Poisson distributions.

Table S1: Comparison of van den Bogaart et al. (30) and our results.

In both van den Bogaart et al. and our experiments, fluorescence increase is observed when fusion occurs (vesicle-vesicle for van der Bogaart et al. and nanodisc-liposome in our case). The absolute values cannot be compared but the variation between 1 SNARE (middle column) and several SNAREs (right column) can. In van den Bogaart et al., the lipid mixing and calcein (content) release are represented by the variation of fluorescence between the initial and final values (taken from Fig. 3b and 5d in this reference). The fraction of liposomes having t-SNARE facing outside is obtained from Fig. 1f and Fig. 2e-bottom panel in van den Bogaart et al. Lipid mixing and content release can then be normalized by this fraction.
In the present study, the end points reported in the "lipid mixing" and "calcum release" raws are obtained from the curves in Fig. 3C and 3D.
When lipid mixing in van den Bogaart et al. is normalized by the fraction of liposomes having t-SNARE correctly oriented, it is exactly the same for one or several SNAREs which is also what we observe. In this reference, the variation of content release also decreases with the number of SNAREs as we observe here but this decrease is not as significant as what we observe. This is probably due to the fact that some of the content is released through an expanded pore.

	Van den Bogaart et al.	
	1 t-SNARE/liposome	20 t-SNAREs / liposome
lipid mixing (%)	6	21
calcein release (%)	2	11
fraction of liposome with t-SNARE facing outside	0.28	1
normalized lipid mixing (%)	21.4	21.0
normalized content release (%)	7.1	11.0
calcein release / lipid mixing	0.33	0.52
	Present study	
	1 v-SNARE/ND	7 v-SNAREs / ND
lipid mixing	25	25
calcium release	3	13
calcium release / lipid mixing	0.12	0.52

Table S2: Comparison of the average numbers of VAMP2 obtained by the various techniques used.

Below are the average numbers of VAMP2 for each nanodisc sample obtained by step-bleaching method, step-bleaching divided by the labeling efficiency (0.9), Coomassie blue and Western blot.

	ND1	ND2	ND4	ND7
Step bleaching	1.2	1.7	2.9	5.1
Normalized step bleaching	1.3	1.9	3.2	5.6
Coomassie blue	1.35	2	4.2	7
Western blot	1.2	2.2	4.3	7.4

References

1. T. C. Südhof, The synaptic vesicle cycle. *Annu. Rev. Neurosci.* **27**, 509 (2004). doi:10.1146/annurev.neuro.26.041002.131412 Medline

2. A. Albillos *et al*., The exocytotic event in chromaffin cells revealed by patch amperometry. *Nature* **389**, 509 (1997). doi:10.1038/39081 Medline

3. L. J. Breckenridge, W. Almers, Currents through the fusion pore that forms during exocytosis of a secretory vesicle. *Nature* **328**, 814 (1987). doi:10.1038/328814a0 Medline

4. D. Bruns, R. Jahn, Real-time measurement of transmitter release from single synaptic vesicles. *Nature* **377**, 62 (1995). doi:10.1038/377062a0 Medline

5. Q. Fang *et al*., The role of the C terminus of the SNARE protein SNAP-25 in fusion pore opening and a model for fusion pore mechanics. *Proc. Natl. Acad. Sci. U.S.A.* **105**, 15388 (2008). doi:10.1073/pnas.0805377105 Medline

6. S. Takamori *et al*., Molecular anatomy of a trafficking organelle. *Cell* **127**, 831 (2006). doi:10.1016/j.cell.2006.10.030 Medline

7. Y. Hu, L. Qu, T. Schikorski, Mean synaptic vesicle size varies among individual excitatory hippocampal synapses. *Synapse* **62**, 953 (2008). doi:10.1002/syn.20567 Medline

8. T. K. Ritchie *et al*., Reconstitution of membrane proteins in phospholipid bilayer nanodiscs. *Methods Enzymol.* **464**, 211 (2009). doi:10.1016/S0076-6879(09)64011-8 Medline

9. J. Frauenfeld *et al*., Cryo-EM structure of the ribosome-SecYE complex in the membrane environment. *Nat. Struct. Mol. Biol.* **18**, 614 (2011). doi:10.1038/nsmb.2026

10. H. Katayama *et al*., Three-dimensional structure of the anthrax toxin pore inserted into lipid nanodiscs and lipid vesicles. *Proc. Natl. Acad. Sci. U.S.A.* **107**, 3453 (2010). doi:10.1073/pnas.1000100107 Medline

11. K. D. Brewer, W. Li, B. E. Horne, J. Rizo, Reluctance to membrane binding enables accessibility of the synaptobrevin SNARE motif for SNARE complex formation. *Proc. Natl. Acad. Sci. U.S.A.* **108**, 12723 (2011). doi:10.1073/pnas.1105128108 Medline

12. T. Weber *et al*., SNAREpins: Minimal machinery for membrane fusion. *Cell* **92**, 759 (1998). doi:10.1016/S0092-8674(00)81404-X Medline

13. C. Hu *et al*., Fusion of cells by flipped SNAREs. *Science* **300**, 1745 (2003). doi:10.1126/science.1084909 Medline

14. T. Söllner *et al*., SNAP receptors implicated in vesicle targeting and fusion. *Nature* **362**, 318 (1993). doi:10.1038/362318a0 Medline

15. R. B. Sutton, D. Fasshauer, R. Jahn, A. T. Brunger, Crystal structure of a SNARE complex involved in synaptic exocytosis at 2.4 A resolution. *Nature* **395**, 347 (1998). doi:10.1038/26412 Medline

16. F. Li *et al*., Energetics and dynamics of SNAREpin folding across lipid bilayers. *Nat. Struct. Mol. Biol.* **14**, 890 (2007). doi:10.1038/nsmb1310 Medline

17. E. A. Smith, J. C. Weisshaar, Docking, not fusion, as the rate-limiting step in a SNARE-driven vesicle fusion assay. *Biophys. J.* **100**, 2141 (2011). doi:10.1016/j.bpj.2011.03.015

18. Y. Xu, F. Zhang, Z. Su, J. A. McNew, Y. K. Shin, Hemifusion in SNARE-mediated membrane fusion. *Nat. Struct. Mol. Biol.* **12**, 417 (2005). doi:10.1038/nsmb921 Medline

19. R. G. Staal, E. V. Mosharov, D. Sulzer, Dopamine neurons release transmitter via a flickering fusion pore. *Nat. Neurosci.* **7**, 341 (2004). doi:10.1038/nn1205 Medline

20. E. N. Pothos, V. Davila, D. Sulzer, Presynaptic recording of quanta from midbrain dopamine neurons and modulation of the quantal size. *J. Neurosci.* **18**, 4106 (1998). Medline

21. R. Khanin, H. Parnas, L. Segel, Diffusion cannot govern the discharge of neurotransmitter in fast synapses. *Biophys. J.* **67**, 966 (1994). doi:10.1016/S0006-3495(94)80562-4 Medline

22. J. A. McNew *et al*., Close is not enough: SNARE-dependent membrane fusion requires an active mechanism that transduces force to membrane anchors. *J. Cell Biol.* **150**, 105 (2000). doi:10.1083/jcb.150.1.105 Medline

23. X. Han, C. T. Wang, J. Bai, E. R. Chapman, M. B. Jackson, Transmembrane segments of syntaxin line the fusion pore of Ca^{2+}-triggered exocytosis. *Science* **304**, 289 (2004). doi:10.1126/science.1095801 Medline

24. E. Fdez, M. Martínez-Salvador, M. Beard, P. Woodman, S. Hilfiker, Transmembrane-domain determinants for SNARE-mediated membrane fusion. *J. Cell Sci.* **123**, 2473 (2010). doi:10.1242/jcs.061325 Medline

25. A. Stein, G. Weber, M. C. Wahl, R. Jahn, Helical extension of the neuronal SNARE complex into the membrane. *Nature* **460**, 525 (2009). Medline

26. J. Kubelka, J. Hofrichter, W. A. Eaton, The protein folding 'speed limit'. *Curr. Opin. Struct. Biol.* **14**, 76 (2004). doi:10.1016/j.sbi.2004.01.013 Medline

27. W. Y. Yang, M. Gruebele, Folding at the speed limit. *Nature* **423**, 193 (2003). doi:10.1038/nature01609 Medline

28. K. A. Dill, S. B. Ozkan, T. R. Weikl, J. D. Chodera, V. A. Voelz, The protein folding problem: When will it be solved? *Curr. Opin. Struct. Biol.* **17**, 342 (2007). doi:10.1016/j.sbi.2007.06.001 Medline

29. E. Karatekin, O. Sandre, F. Brochard-Wyart, Transient pores in vesicles. *Polym. Int.* **52**, 486 (2003). doi:10.1002/pi.1007

30. G. van den Bogaart *et al*., One SNARE complex is sufficient for membrane fusion. *Nat. Struct. Mol. Biol.* **17**, 358 (2010). doi:10.1038/nsmb.1748 Medline

31. Y. Hua, R. H. Scheller, Three SNARE complexes cooperate to mediate membrane fusion. *Proc. Natl. Acad. Sci. U.S.A.* **98**, 8065 (2001). doi:10.1073/pnas.131214798 Medline

32. R. Mohrmann, H. de Wit, M. Verhage, E. Neher, J. B. Sørensen, Fast vesicle fusion in living cells requires at least three SNARE complexes. *Science* **330**, 502 (2010). doi:10.1126/science.1193134 Medline

33. C. Montecucco, G. Schiavo, S. Pantano, SNARE complexes and neuroexocytosis: How many, how close? *Trends Biochem. Sci.* **30**, 367 (2005). doi:10.1016/j.tibs.2005.05.002 Medline

34. T. Lang *et al*., SNAREs are concentrated in cholesterol-dependent clusters that define docking and fusion sites for exocytosis. *EMBO J.* **20**, 2202 (2001). doi:10.1093/emboj/20.9.2202 Medline

35. T. J. Melia *et al*., Regulation of membrane fusion by the membrane-proximal coil of the t-SNARE during zippering of SNAREpins. *J. Cell Biol.* **158**, 929 (2002). doi:10.1083/jcb.200112081 Medline

36. J. Shen, D. C. Tareste, F. Paumet, J. E. Rothman, T. J. Melia, Selective activation of cognate SNAREpins by Sec1/Munc18 proteins. *Cell* **128**, 183 (2007). doi:10.1016/j.cell.2006.12.016 Medline

37. N. S. Heyman, J. M. Burt, Hindered diffusion through an aqueous pore describes invariant dye selectivity of Cx43 junctions. *Biophys. J.* **94**, 840 (2008). doi:10.1529/biophysj.107.115634 Medline

38. E. Karatekin *et al*., A fast, single-vesicle fusion assay mimics physiological SNARE requirements. *Proc. Natl. Acad. Sci. U.S.A.* **107**, 3517 (2010). doi:10.1073/pnas.0914723107 Medline

39. E. A. Permiakov, *Metalloproteomics* (Wiley, Hoboken, NJ, 2009).